

56606

MOLECULAR-DYNAMICS COMPUTER SIMULATION
OF COPPER CLUSTERS:
STRUCTURAL STABILITY, ENERGETICS, AND MELTING

A THESIS SUBMITTED TO
THE GRADUATE SCHOOL OF NATURAL AND APPLIED SCIENCES
OF
THE MIDDLE EAST TECHNICAL UNIVERSITY

BY

CEM ÖZDOĞAN

IN PARTIAL FULFILLMENT OF THE REQUIREMENTS FOR THE DEGREE OF
MASTER OF SCIENCE
IN
THE DEPARTMENT OF PHYSICS

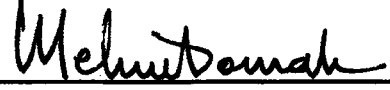
AUGUST 1996

Approval of the Graduate School of Natural and Applied Sciences.



Prof. Dr. Tayfur Öztürk
Director

I certify that this thesis satisfies all the requirements as a thesis for the degree of Master of Science.



Prof. Dr. Mehmet Tomak
Head of Department

This is to certify that we have read this thesis and that in our opinion it is fully adequate, in scope and quality, as a thesis for the degree of Master of Science.



Prof. Dr. Şakir Erkoç
Supervisor

Examining Committee Members

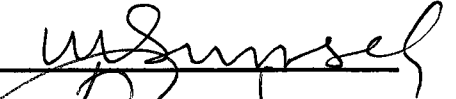
Prof. Dr. Şakir Erkoç



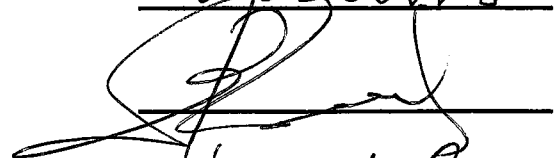
Prof. Dr. Ramazan Sever



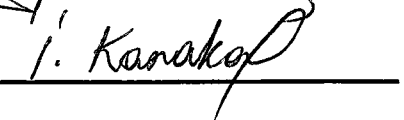
Prof. Dr. Mehmet Şimşek



Prof. Dr. Lemi Türker



Prof. Dr. İshak Karakaya



ABSTRACT

MOLECULAR-DYNAMICS COMPUTER SIMULATION OF COPPER CLUSTERS: STRUCTURAL STABILITY, ENERGETICS, AND MELTING

Özdoğan, Cem

M.S., Department of Physics

Supervisor: Prof. Dr. Şakir Erkoç

August 1996, 115 pages.

We have investigated cluster properties of copper using the Molecular-Dynamics technique. In the simulation an empirical potential energy function (PEF) proposed by Erkoç has been used, which contains two-body atomic interactions. The structural stability and energetics of Cu_n ($n = 13 - 135$) shell like structured clusters have been investigated at temperatures $T = 1\text{ K}$ and $T = 300\text{ K}$. It has been found that the average interaction energy per atom in the cluster decreases and reaches an asymptotic value as cluster size increases. The melting behaviour of clusters $n = 13$ and $n = 55$ have been investigated. It has been found that the melting temperature decreases as cluster size increases, and for clusters with multishell structures melting starts from the outermost shell. The present results are qualitatively in agreement with available literature values.

Keywords: Cluster, Molecular-Dynamics Simulation, Verlet Algorithm, Empirical Many-Body Potential Energy Function, Maxwell Velocity Distribution.

ÖZ

BAKIR "CLUSTER"LARININ MOLEKÜLER-DİNAMİK BİLGİSAYAR SİMÜLÂSYONU: KARARLI YAPILARI, ENERJİLERİ VE ERİMESİ

Özdoğan, Cem

Yüksek Lisans , Fizik Bölümü

Tez Yöneticisi: Prof. Dr. Şakir Erkoç

Ağustos 1996, 115 sayfa.

Moleküler-Dinamik bilgisayar simülasyonu metodu ile bakırın "cluster"-larının özellikleri incelendi. Simülasyonda Erkoç tarafından teklif edilen ikili atomik etkileşmelerden oluşan ampirik bir potansiyel enerji fonksiyonu kullanıldı. Cu_n ($n = 13 - 135$) küresel kabuk şeklinde yapılmış "cluster"ların yapıları ve enerjileri $T = 1 K$ ve $T = 300 K$ sıcaklıklarında incelendi. "Cluster"ların büyüklüklerinin artmasıyla ortalama atom başına düşen etkileşme enerjisinin asimtotik olarak düştüğü görülmüştür. $n = 13$ ve $n = 55$ "cluster"larının erimesi incelendi. "Cluster" büyüklüğünün artmasıyla erime sıcaklığının düştüğü ve çok kabuklu yapılarda erimenin en dıştaki kabuktan başladığı görülmüştür. Elde edilen sonuçlar mevcut literatür değerleri ile uyum içindedir.

Anahtar Kelimeler: "Cluster", Moleküler-Dinamik Simülasyonu, Verlet Yöntemi, Ampirik Çok-Cisim Potansiyel Enerji Fonksiyonu, Maxwell Hız Dağılımı.

ACKNOWLEDGMENTS

I am deeply thankful to Prof. Dr. Şakir Erkoç as a supervisor for his valuable guidance and his continued encouragement and suggestions throughout all stages of my M.S. study .

I am also grateful to Abdullah Göksu and Eren San for their honourable companions, worthy supports and encouragements during these stages.

I am also thankful to Serkan Çelepken for his technical support.



TABLE OF CONTENTS

ABSTRACT	iii
ÖZ	iv
ACKNOWLEDGMENTS	v
TABLE OF CONTENTS	vi
CHAPTER	
1 INTRODUCTION	1
1.1 Definitions and classifications	4
1.1.1 Classification with respect to composition	5
1.1.2 Classification with respect to surroundings	5
1.1.3 Classification with respect to size	6
1.1.4 Classification with respect to level structures	7
1.2 Formation, characterization and investigation methods	7
1.2.1 Nature's Way	7
1.2.2 Generation	8
1.2.3 Characterization techniques	11
1.2.4 Ab initio methods	14
1.2.5 Semi-empirical methods	15
1.3 Important properties of small clusters	16
1.3.1 Structural and electronic properties	16
2 THE POTENTIAL ENERGY FUNCTION	20
2.1 Born–Oppenheimer approximation	20
2.2 Erkoç PEF	22

3	COMPUTER SIMULATION METHODS	26
3.1	Historical background	26
3.1.1	Early days	26
3.1.2	New methods appeared in the 1980s	29
3.2	Simulation in Cluster research	29
3.3	Ensembles	31
3.3.1	Canonical–Ensemble Averages	32
3.4	Molecular Dynamics (MD)	34
3.4.1	Molecular Dynamics Averages	35
3.4.2	Approach to Equilibrium	37
3.4.3	Time–Saving Techniques	38
3.5	Monte Carlo (MC)	42
3.6	Energy minimization (EM)	44
4	CALCULATIONS & RESULTS	49
4.1	Shell–like Copper Clusters	49
5	CONCLUSION & DISCUSSION	92
	REFERENCES	96
A	ACRONYMS	101
B	MAXWELL–BOLTZMANN VELOCITY DISTRIBUTION	103
B.1	The distribution of molecular velocities	103
B.2	Algorithm for Maxwell Velocity Distribution	108
C	ALGORITHM AND FLOWCHART OF THE PROGRAM	111
C.1	Algorithm	111
C.2	Flowchart	113
D	DETERMINATION OF ΔT	114

LIST OF TABLES

TABLE

2.1	Parameters of the PEF for copper [45]. In the determination of the PEF parameters energy was taken in eV and distance was taken in Å.	25
4.1	Total number of atoms in the cluster with respect to shell size.	50
4.2	Initial radius d_{nn} of fcc spherical clusters and calculated average radii (in Å) $r_1, r_2, r_3, r_4, r_5, r_6$ and r_7 at $T = 1 K$	59
4.3	Initial radius d_{nn} of fcc spherical clusters and calculated average radii (in Å) $r_1, r_2, r_3, r_4, r_5, r_6$ and r_7 at $T = 300 K$	59
4.4	The average interaction energy per atom (in eV), Φ/n , in Cu_n clusters for Ideal and at $T = 1 K, T = 300 K$	74
4.5	Calculated melting points for $n = 13, n = 55$ clusters and inner shells of $n = 55$ cluster.	88
5.1	The ratios of average interaction energy per atom for Cu_n ($n = 13, 55, 79$) clusters.	94

LIST OF FIGURES

FIGURES

2.1	The potential profiles of a) pair potential, and b) effective pair potential. $E_0 = -2.035$ eV, $E'_0 = -0.22$ eV, $r_0 = 2.22$ Å, and $r'_0 = 2.74$ Å.	24
3.1	Time evolution of a dynamical system.	38
3.2	Energy (E) minimization with respect to some structural variable x . The system runs down from the starting point S to the minimum M.	46
3.3	Illustration of the local minimum problem with the system running from S to the local minimum L, despite the presence of lower global minimum G.	48
4.1	Potential Energy (in eV) vs MD steps for $n = 13$ cluster at $T = 1$ K and $T = 300$ K.	52
4.2	Potential Energy (in eV) vs MD steps for $n = 19$ cluster at $T = 1$ K and $T = 300$ K.	53
4.3	Potential Energy (in eV) vs MD steps for $n = 43$ cluster at $T = 1$ K and $T = 300$ K.	54
4.4	Potential Energy (in eV) vs MD steps for $n = 55$ cluster at $T = 1$ K and $T = 300$ K.	55
4.5	Potential Energy (in eV) vs MD steps for $n = 79$ cluster at $T = 1$ K and $T = 300$ K.	56
4.6	Potential Energy (in eV) vs MD steps for $n = 87$ cluster at $T = 1$ K and $T = 300$ K.	57
4.7	Potential Energy (in eV) vs MD steps for $n = 135$ cluster at $T = 1$ K and $T = 300$ K.	58
4.8	Radial Distribution Function vs Distance (in Å) for $n = 13$ cluster at Ideal, $T = 1$ K and $T = 300$ K.	60
4.9	Radial Distribution Function vs Distance (in Å) for $n = 19$ cluster at Ideal, $T = 1$ K and $T = 300$ K.	61
4.10	Radial Distribution Function vs Distance (in Å) for $n = 43$ cluster at Ideal, $T = 1$ K and $T = 300$ K.	62
4.11	Radial Distribution Function vs Distance (in Å) for $n = 55$ cluster at Ideal, $T = 1$ K and $T = 300$ K.	63

4.12	Radial Distribution Function vs Distance (in Å) for $n = 79$ cluster at Ideal, $T = 1 K$ and $T = 300 K$	64
4.13	Radial Distribution Function vs Distance (in Å) for $n = 87$ cluster at Ideal, $T = 1 K$ and $T = 300 K$	65
4.14	Radial Distribution Function vs Distance (in Å) for $n = 135$ cluster at Ideal, $T = 1 K$ and $T = 300 K$	66
4.15	Structures for $n = 13$ cluster at Ideal, $T = 1 K$ and $T = 300 K$	67
4.16	Structures for $n = 19$ cluster at Ideal, $T = 1 K$ and $T = 300 K$	68
4.17	Structures for $n = 43$ cluster at Ideal, $T = 1 K$ and $T = 300 K$	69
4.18	Structures for $n = 55$ cluster at Ideal, $T = 1 K$ and $T = 300 K$	70
4.19	Structures for $n = 79$ cluster at Ideal, $T = 1 K$ and $T = 300 K$	71
4.20	Structures for $n = 87$ cluster at Ideal, $T = 1 K$ and $T = 300 K$	72
4.21	Structures for $n = 135$ cluster at Ideal, $T = 1 K$ and $T = 300 K$	73
4.22	The variation of average interaction energy per atom, $\Phi = \Phi/n$, as a function of the cluster size.	75
4.23	The variation of average interaction energy, E_b (in eV), as a function of temperature for $n = 13$ cluster by using model1.	79
4.24	The variation of average interaction energy, E_b (in eV), as a function of temperature for $n = 13$ cluster by using model2.	80
4.25	The variation of average interaction energy, E_b (in eV), as a function of temperature for $n = 55$ cluster by using model1.	81
4.26	The distortions in structure for $n = 13$ cluster between $T = 900 K$ and $T = 1500 K$	82
4.27	The distortions in structure for $n = 13$ cluster between $T = 3900 K$ and $T = 4500 K$	83
4.28	The distortions in structure for $n = 55$ cluster between $T = 300 K$ and $T = 1200 K$	84
4.29	The distortions in structure for $n = 55$ cluster between $T = 3900 K$ and $T = 6900 K$	85
4.30	Standard Deviation (σ) versus Temperature (in K) for $n = 13$ cluster.	86
4.31	Standard Deviation (σ) versus Temperature (in K) for $n = 55$ cluster.	87
4.32	Standard Deviations of N_1 of $n = 55$ cluster versus Temperature (in K).	89

4.33 Standard Deviations of N_2 of $n = 55$ cluster versus Temperature (in K).	90
4.34 Standard Deviations of N_3 of $n = 55$ cluster versus Temperature (in K).	91
B.1 Diagram of velocity space.	105
B.2 Graph of Maxwell–Boltzmann speed distribution function. . .	107
B.3 Most probable (v_m), arithmetic mean (\bar{v}), and the root-mean-square (v_{rms}) speeds.	108



CHAPTER 1

INTRODUCTION

Today, not only the catalytic chemists, but also scientists from many other disciplines are involved with studies related to small clusters. This field constitutes one of the important areas where experiments and theoretical work go hand in hand and benefit considerably from each others' results. Because the characterization of microclusters is believed to furnish additional information about the fundamental mechanism of catalysis and many important chemical reactions, properties of small clusters, have become a subject of intense theoretical and experimental investigations [1]. This growing interest is at present not only a technological one, but also has established academic roots. Since small-cluster research is involved with microscopic level, investigations, the results that it produces are extremely valuable in the understanding of various very important processes. There are some compelling reasons for the study of clusters [2];

i– Exploration of new basic physical phenomena. These are finite systems with a congested spectrum of energy levels (for electronic states, phonons, etc.). The level structure can be varied continuously by changing the cluster

size. Accordingly, one can accomplish a 'continuous transition' from molecular to solid-state systems,

ii– Microscopic approach to macroscopic phenomena, such as nucleation, adsorption and desorption and catalysis,

iii– A variety of technological applications rests on cluster physics and chemistry. These include photography, aerosols and smoke, sintering of small particles in vacuum, plasma injection, as well as magnetism and superconductivity of metallic clusters,

iv– Astrophysical applications. The elucidation of the nature, the formation mechanism and the properties of cosmic dust rests on cluster science.

Atoms in a microcluster have, in general, different surroundings with respect to those in the bulk state. For example, the average number of nearest neighbors of an atom in a cluster does not always correspond to its chemical valance, and it differs also from the number of nearest neighbors in the corresponding crystal [3]. Many quantities (such as the temperature, surface tension, surface area and even the volume) that are used in the description of macroscopic systems become ill defined as the cluster size decreases. Therefore, in the classical nucleation approach, for instance, one encounters many difficulties in calculating properties of small clusters from thermodynamical considerations [4, 5]. While the contribution coming from atoms located at surfaces to many intensive properties is negligible in the description of a macroscopic system, it plays an important part in the case of small clusters.

The most popular question asked in microcluster work is: how do the

different material properties vary as function of the cluster size? Today, it is well known that many characteristics associated with small clusters vary non-monotonically going from a dimer to the bulk state. For example, intriguing variations in the chemical reactivity and selectivity are the two significant features over which the catalytic chemist would like to obtain complete control. Microclusters display curious crystallographic anomalies which cannot be found in the bulk. Pentagonal structures exist for small dimension phases. Energy and stability calculations show that these structures are energetically favoured when they are compared to normal bulk structures. In many instances, researches dealing with small clusters which looked like an amorphous structures [6, 7]. Electronic excitations and ionization characteristics of microclusters were also found to be quite different from respective processes in the bulk [8, 9]. Undoubtedly, a thorough understanding an enormous advantage in manipulating various technologically important reactions in the directions desired. From an academic viewpoint, on the other hand, the evolution of the structural, electronic and other properties as atoms form progressively larger clusters leading to a macroscopic-size solid has long been a challenging problem for solid state and theoretical physicists. An enormous amount of experimental and theoretical work has been conducted to resolve how these various properties of the solid state evolve. These intensified efforts, during the last decade in particular, have resulted in an overwhelming advancement in microcluster research. Today, clusters (neutral or ionic) can be generated from practically any element. Characterization techniques have

been developed to such a state that for structural identifications in a variety of cases atomic-level resolutions are possible. Very fundamental steps have been taken toward the understanding of chemical reactivity. The availability of supercomputers, on the hand, furnished tremendous help in understanding microcluster properties via accurate *ab initio* calculations along with detailed computer simulation methods. Their contribution to small-cluster research is at present making an impact by providing atomistic level information (unavailable by experimental means) to solve many problems related to stability and other structural properties. Theoretical methods along with the atomistic computer simulation techniques are on their way to becoming an integral part of the characterization procedures by providing sound models and contributing to the interpretation of many experimental observations [10].

1.1 Definitions and classifications

Microclusters may be defined as aggregates of atoms (or molecules) held under different conditions. In general, it is anticipated that properties of microclusters are different from their bulk- or crystalline-state properties. A precise description of microclusters may be achieved by using four different classification schemes based on the composition, surroundings, size and the level structure of the cluster.

1.1.1 Classification with respect to composition

In this scheme clusters may be categorised into two parts as homonuclear and heteronuclear clusters. Homonuclear clusters are monatomic systems and constitute the simplest category. They are used very frequently in small-cluster research because of their importance in understanding the general behaviour of microclusters. Heteronuclear, on the other hand, include alloys and molecular species. The types of atoms which constitute a cluster are perhaps most important factors responsible for cluster characteristics. The composition reflects the types of bondings (such as covalent, metallic, van der Waals, etc.) and interactions operational among the atoms in the cluster. While in the case of a homonuclear cluster only one type of interaction is expected, for heteronuclear cases different types of bonding combinations may exist.

1.1.2 Classification with respect to surroundings

Environmental effects on properties of microclusters may be quite significant. In this respect clusters may be reviewed in two basic categories: isolated clusters and trapped clusters. Isolated clusters are those with no (or negligible) environmental influence acting upon them. In general, gas-phase clusters under low-pressure conditions may be included in this group. In this case, of course, forces operational among the clusters in the gas phase, as well as interactions between the carrier-gas molecules and the clusters,

should be negligible. Because of the need to understand many specific properties associated with microclusters and to sort out environmental effects, isolated small-clusters research has gained tremendous momentum during the last two decades. Trapped clusters, on the other hand, were the subject of many earlier effects (produced by interactions between the cluster atoms and the neighbouring atoms of the support) which might have altered various physical and chemical properties of the cluster with respect to its isolated condition. Examples for trapped clusters include clusters in matrices, in zeolites, in polymers, in solutions, or clusters deposited on substrate surfaces.

1.1.3 Classification with respect to size

One of the most common classification schemes for microclusters is that based on size. In general, very small clusters are defined as those containing 2 – 10 atoms and this group of clusters are usually called as microclusters; small-size clusters are those with $10-10^2$ atoms; medium size clusters contain $10^2 - 10^3$ atoms; large clusters have $10^3 - 10^4$ atoms while clusters containing more than 10^5 atoms are classified very large clusters. Even though the boundaries in this classification scheme are somewhat arbitrary and depend very much on the type of atomic species involved, there are many differences not only in properties of clusters in going from one group to the other, but also in their preparation and characterization techniques as well. While properties of clusters in the very-large-size group resemble bulk properties, many

characteristics of very-small-size and small-size clusters deviate sharply from their bulk values.

1.1.4 Classification with respect to level structures

In their description of microclusters, the thermodynamic and electronic states of particles play an important role. In this classification scheme, in general, clusters may be grouped in two categories, namely neutral and ionic species. Most of the small-cluster research is involved with neutral particles which are often assumed to be in their ground state. However, for characterization purposes, in many of the gas-phase experiments in particular, clusters in their higher (rotational, vibrational and electronic) levels of excitations are used. In this respect, melted clusters, for instance, may be classified as thermally excited neutral particles. In gas-phase cluster experiments negatively or positively charged particles are used primarily. Single or multiple ionization of particles is utilized in association with various characterization and separation techniques in isolated small-cluster research.

1.2 Formation, characterization and investigation methods

1.2.1 Nature's Way

At that point, the question of 'What is the Nature's way of producing clusters?' may be asked. The history of the expanding universe abounds with examples of cluster formation, as expansion and cooling has taken matter in

the initial cosmic fireball through various steps. During the first epoch, lasting a fraction of a second, quarks clustered together in groups of three to make nucleons. Much later, the nucleons joined together to form nuclei with up to a hundred protons and one hundred and fifty neutrons. This took place in the gas mantle, expanding outwards from the hot star, electrons were subsequently aggregating around the nuclei. This was due to their own cohesion but because of the electrical attraction from the positively charged nuclei. Therefore the aggregation is limited to the number of electrons needed to balance the number of protons in the nucleus.

These are special, though important, examples. In these cases the clustering process terminates at a definite maximum size. There are of course many other examples of clustering without such bounds, for instance into molecules, dust particles, raindrops and even planets or stars [11].

1.2.2 Generation

Among the methods of producing small clusters, condensation in free jets is the most widely used technique in generating gas-phase microclusters. Generation of isolated small clusters in their 'equilibrium' morphology, free of environmental effects and for a time period allowing proper separation and identification, is a challenging problem even for permanent gases or van der Waals systems. In general, the thermodynamic state of the gas prior to its expansion and the nozzle dimensions determine the cluster characteristics. For producing cluster beams for a metal (or semiconductor), the material

must be heated well above its melting point to obtain vapour pressure high enough for a dynamic expansion. Metal clusters and the carrier gas then pass through a nozzle into a fast flow–reaction channel to form the cluster beam as the mixture flows into a vacuum [12]. Another technique called ‘multiple expansion cluster source’, which is used to produce microclusters of metals, has been employed by Bowles *et al* [13]. These researchers were able to form clusters of Cu, Ag, Au and Ni as an aerosol supported in an inert gas which is then expanded through a hole into a vacuum chamber where the cluster beam is formed.

For generating ions, the clusters in the beam are ionised by electron impact or by laser photons to produce positively charged particles, or an electron attachment method must be used for obtaining negatively charged particles before they reach the detection chamber. Also, cluster ions may be produced from ionic gaseous atoms (or molecules) which subsequently undergo clustering reactions [14]. Another method to produce ionised particles uses a liquid–metal ion source (LMIS). In this technique a liquid meniscus of a metal is submitted to a very intense electric field that produces a beam of charged particles [15].

In general, two problems are associated with cluster beam generation techniques: the first is the difficulty of preparing a sample of specific cluster size with adequate purity and abundance, and the second is the limited time available for the observation of clusters in the generated beam. The latter problem is related to the thermodynamic state of the particles in the beam. In

order to overcome the difficulty mentioned above and to obtain more specific information about the stability and size of clusters in the beam studies, a separation step is introduced prior to the final detection step. In general, separation of clusters in the beam is a difficult problem. For separation of ionic clusters the most popular method is a combined technique which involves ionization and mass separation steps. It is, however, cumbersome to use this method for producing neutral clusters because it should contain an additional neutralization step for the ionic species.

Other methods, which are best suited for smaller size clusters, employ beam deflection procedures. These methods are based on magnetic-, electric-, crossjet- or photo-deflection techniques and do not involve ionization steps [16, 17, 18]. Some of these techniques for generating a neutral, mass-selected cluster beam have been examined by Arnold *et al* [19].

Another procedure to prepare microclusters for further investigations is the matrix isolation technique. In this method microclusters are trapped in a solid environment. To eliminate or rather minimize undesired environmental effects due to the cluster-matrix interaction, in general matrices of rare-gas solids are utilised in this technique. The process of the matrix isolation of clusters involves a step of co-condensing a vapour with a rare gas onto a cold surface. In the earlier matrix isolation techniques it has been assumed, in general, that trapped clusters conserve their gas-phase properties and that the interaction between the atoms in the clusters and the surrounding

matrix is negligible. Also, for the preparation of the small- to intermediate-size clusters, seeded beam or gas-aggregation techniques (based on a liquid-helium-cooled differential pumping), which provide a narrow size distribution of the particles, are employed [20].

For the preparation of microclusters supported on substrates, the most commonly used technique is vapour deposition. Many experimental techniques have been developed for the preparation as well as for the characterization of substrate-deposited small clusters. Most of these experiments were performed for model catalytic studies with UHV-evaporated metal clusters. Results indicate that the crystallinity, cleanliness, stoichiometry and structural perfection of the support surface play a major role in determining the structural properties of the cluster.

1.2.3 Characterization techniques

In general, for the characterization of microclusters, the above preparation procedures are coupled with one or more identification techniques and constitute one single integrated characterization experiment.

Time-of-flight mass spectrometry (TOFMS) is an important technique which is used quite frequently for the analysis of gas-phase-generated small clusters during the time of their flight from the reaction chamber to the vacuum. Multiphoton ionization spectroscopy is another very useful technique for the characterization of small clusters in supersonic jets. In this technique,

first, one or more photons are tuned into resonance with an electronic transition, exciting a bound state of the neutral particle. Then, an additional photon excites the particle to its ionization, producing a cation [17, 21].

Photodetachment and photoelectron spectroscopy have proved to be powerful methods for the characterization of some small-cluster negative ions. Basic principles of the photodetachment of negative ions have been well documented by Feigerle *et al* [22] and Stevens *et al* [23]. In these measurements the temperature of the cluster ion and, photofragmentation, are among the experimental problems cited. Structural characterization methods based on electron diffraction techniques are among the most effective experimental tools available for research on clusters. For crystalline clusters it can often determine in detail the atomic arrangement, cluster size and density. For amorphous or liquid-like clusters, however, the diffraction information is somewhat more limited. It has been shown that computer simulation studies now can provide supplementary evidence of considerable value for filling in details not resolved by the diffraction analysis [24].

Among the x-ray techniques (EXAFS) is the most widely used technique for structural characterization of small clusters deposited on substrate surfaces, carbon films and for microparticles trapped in zeolites or matrices [25, 26, 27]. In general, (EXAFS), which requires synchrotron radiation, provides an accurate

Another important technique to determine the structure and morphology of supported clusters is the radial electron distribution method which based

based on x-ray scattering measurements. (RED) provides the complete set of interatomic distances present in the cluster as opposed to (EXAFS) which probes mainly the first coordination sphere around the absorbing atom. These techniques have been compared in articles by Poppa [26] and Gallezto [27]. Many of the techniques developed for analysis of crystalline surfaces have been adapted for the characterization of supported clusters. In supported small-cluster research (such as in model studies on catalysis) (UHV)-based integrated devices are being used for characterisation as well as for preparation purposes. One of the most important advantages of such integrated techniques is to provide an excellent analytical environment, including high-energy-resolution/highsensitivity electron and infrared spectroscopy methods and high-spatial-resolution electron microscopy (and diffraction) to characterise the system in great detail [26]. Furthermore, (UHV)-integrated techniques can also furnish the highly desired control of the cleanliness of the experimental environment that is necessary for the stoichiometry and morphology of the substrate surfaces as well as for the structure, size and the habit for the supported particles.

Many of the techniques for probing bulk surfaces are also used for the study of supported small clusters. Recent techniques employed in characterization studies of supported clusters can broadly be classified in two groups. (i) High spatial resolution techniques that have limited analytical power; these include micro-area electron diffraction, TEM, STEM, STED. (ii) Large-area methods are based on various spectroscopic and diffraction techniques

as well as thermal desorption and workfunction measurements (such as UPS, XPS, LEED, SIMS, TPD, EXAFS, AES). Often two or more of these techniques are combined to form powerful experimental approaches [26]. The most commonly used integrated experimental techniques in supported cluster research include the TPD/AES dual-chamber system [28], the XPS/AES/WF/TPD system [26], the UHV *in situ* TEM/TED stage [29, 30] and the UHV *in situ* STED system [26, 31].

1.2.4 Ab initio methods

The *ab initio* methods loosely divide into the SCF/MCSCF/CI, or molecular orbital (MO), and density functional approaches. The MO approaches have proven to yield extremely accurate results for small molecules; in many cases rivalling the accuracy possible in experiments. With the current methods and supercomputers, the size of the system that can be treated is large compared to a decade ago. However, MO methods suffer from the rapid growth in work with problem size. Hence the system size increases it is common to make more approximations either in the orbital basis set or in the treatment of correlation. Both of these approximations naturally reduce the accuracy of the method. The density functional approaches were developed based upon the assumption that the exchange and correlation energies can be approximated by functions of the electron density. This approximation greatly reduces the work relative to the MO methods. The local spin density version of this approach appears to yield a reliable view of metals [32], and

thus suggests that the approximation is quite good.

The applicability and associated level of success of different *ab initio* methods in predicting properties of small to very small clusters of atoms have shown enormous improvements during the last ten years[10].

1.2.5 Semi-empirical methods

Semi-empirical methods, in general, starts with the basic ideas used in *ab initio* methods, but reduce the complexity by many approximations. They further reduce the work by approximating many of the required matrix elements with information deduced from experiment. The parameters used to approximate the matrix elements can be fine tuned, based upon application of the method to molecular systems for which experimental data exists. It is probably not surprising that for a series of n related compounds, if the semi-empirical methods are calibrated for $n-1$, they can do quite well for the n th; in general, this appears to be the case for organic systems where many well understood examples can be used to calibrate the methods. It is not clear how to extend the semi-empirical methods to the study of the reactions of the metal clusters. It appears that some caution must be used in applying semi-empirical methods to interpret the chemistry of metal clusters. It is hoped that as more experimental and accurate *ab initio* data become available to calibrate these methods their reliability and applicability will increase.

1.3 Important properties of small clusters

One of the most significant and popular features of small-cluster investigation is the analysis of various properties as a function of cluster size. Any property associated with a small cluster is expected to converge to its parent bulk value as the cluster size approaches macroscopic dimensions. In many studies (experimental and theoretical) it has been clearly demonstrated that this convergence has a non-monotonic character and has different slopes for different properties. Depending on the atomic species, involved deviations from the linearity in cluster properties are most pronounced in the very-small- and small-size cluster regions. In general, structural and electronic properties as well as magnetism and energetics of clusters are very closely interconnected and therefore it is difficult to analyse them independently [33]. While the positions of atomic nuclei in a microcluster determine the electronic states, the distribution of electrons, in turn, plays an important role in energetics; accordingly, it affects the shape and the overall geometry of the cluster along with its magnetic quality.

1.3.1 Structural and electronic properties

Unfortunately, detailed configurational analysis of a cluster on an atomic scale is a very difficult task. For gas-phase clusters, in general, structural information comes from electron diffraction studies. For trapped clusters,

on the other hand, techniques such as EXAFS along with electron diffraction techniques are employed. While for trapped clusters structural property measurement can be conducted at leisure, one faces difficulties in analysing and sorting out associated environmental effects due to interaction between the atoms in the cluster and the surrounding atoms. In the case of gas-phase clusters, on the other hand, the environmental effect is minimal. However, the timing of the measurement is often restricted, depending on the type of the experimental technique and equipment utilised. In general, the time lapse between the generation of a cluster in the gas phase and the measurement step is quite short, therefore findings related to the stability of small clusters and their equilibrium conditions are open to various criticisms [21, 34]. The equilibrium condition is an important consideration in correlating the abundance ratio of a particular species in the beam with its stability. Since different size clusters may dissociate (or associate) at different rates, the abundance ratio in the beam at a non equilibrated state may not always reflect the stability of gas-phase clusters at their equilibrated state.

Theoretical investigations indicate that small clusters exhibit different geometrical structures with varying degrees of symmetry corresponding to metastable states which, in many cases, are nearly degenerate with the ground-state configuration. Two important conclusions may be drawn from theoretical investigations on the structure and stability of microcluster. (i) In general, a number of different stable structures are likely be found energetically in near degeneracy with the ground-state configuration. (ii) The

energetically lowest configuration does not have to be associated with a three-dimensional high-symmetry structure.

The first conclusion mentioned above can be recognised as the main cause of the fluxional nature of the small clusters that produces an additional difficulty in the structural determination of isolated small clusters. In general, it is anticipated that fluxionality of clusters is inversely proportional to its size. In the structural characterization of microclusters, bond length measurements play an important role. In the majority of the experimental studies, it has been found that the nearest-neighbour distance contracts as the cluster size decrease.

Thermodynamic properties such as the melting point and the vapour pressure of microclusters also display considerable deviations as a function of cluster size. For smaller-size clusters vapour pressure increases as the melting point drops. As Poppa [26] outlined in his review, such important thermodynamic property variation associated with cluster dimensions must be taken into consideration in the context of sintering and dispersion studies in the supported cluster research. In computer simulation studies it has been found that in the smaller size regimes a temperature interval ΔT_c , exists where solid-like and liquid-like structures can coexist [35, 36]. This temperature interval was defined as $\Delta T_c = T_m - T_f$ where T_m denotes the upper bound of stability for the solid and T_f is the lower bound of stability for the liquid. Beck [35] found that ΔT_c is not a simple function of the cluster size, but generally increases as the size increases. Other computer simulation

investigations [37, 38, 39, 40] on the melting properties of rare gas clusters indicate that, in general, melting behaviour exhibits strong dependence on the size of the cluster.



CHAPTER 2

THE POTENTIAL ENERGY FUNCTION

2.1 Born–Oppenheimer approximation

The Born–Oppenheimer approximation [41] provides an unambiguous definition of a potential energy function for the nuclei which depends only upon their positions and implicitly contains the energy of the ground state electronic wave functions that binds them together. If there are no external fields acting on the system, then this potential depends on the relative positions of the nuclei. If it is assumed that a function $\Phi(\mathbf{r}_1, \dots, \mathbf{r}_N)$ exists to describe the total potential energy of an isolated system of N atoms as a function of their positions, then without any loss of generality the function Φ can be expanded as [42],

$$\Phi = \varphi_2 + \varphi_3 + \dots + \varphi_n + \dots \quad (2.1)$$

where $\varphi_2, \varphi_3, \dots, \varphi_n$ represents two-, three-, ... and n -body potentials respectively. In an explicit form

$$\Phi = \sum_{i < j}^N u(\mathbf{r}_i, \mathbf{r}_j) + \sum_{i < j < k}^N u(\mathbf{r}_i, \mathbf{r}_j, \mathbf{r}_k) + \dots + \sum_{i < \dots < n}^N u(\mathbf{r}_i, \dots, \mathbf{r}_n) + \dots \quad (2.2)$$

where $u(\mathbf{r}_i, \mathbf{r}_j)$, $u(\mathbf{r}_i, \mathbf{r}_j, \mathbf{r}_k)$ and $u(\mathbf{r}_i, \dots, \mathbf{r}_n)$ denote the two-body, three-body and n -body interactions, respectively. In this so-called many-body

expansion of Φ , it is usually believed that the series has a quick convergence, therefore the higher moments may be neglected [43, 44]. Otherwise this equation cannot be employed for systems containing more than only a few atoms.

In the earlier calculations, in general, the higher terms including even the three-body part were omitted, and the total potential energy, Φ was approximated only by the sum of two-body interactions. This approach, which may be regarded as a first-order approximation, not only simplified the statistical mechanical formalism used in calculating various thermodynamical properties, but, more importantly, it enabled many earlier researchers to run simulation calculations with relatively smaller and less powerful computers. In most of the simulation calculations which are carried out considering this first-order approximation, Lennard-Jones type functions were employed to mimic two-body interactions. Despite the fact that those so-called Lennard-Jones systems may represent only microclusters of rare gases where the role of many-body forces are minimal, they provided a very useful understanding about many properties of microclusters in a systematic way that could not be acquired easily by other means. However, particularly in the case of systems containing atoms other than those with close-shell structures, this first-order approximation is inappropriate and produces results inconsistent with many experiments due to neglect of many-body interactions. Therefore, in addition to two-body interactions, three-body interactions also are being considered in the calculation of potential energies. As anticipated, the type

of potential energy function used in a modelling procedure dictates many properties of small clusters, such as the stability and the energetics and, of course, the distribution of the configurational energy levels, as well.

2.2 Erkoç PEF

The PEF that we used in our work contains only two-body interactions terms to make the simulations easy for many-particle systems [45]. The contribution of the truncated terms may be included by inserting linear combination parameters to the remaining terms. In this form one can insert one linear parameter into the total PEF. However, one may insert parameters into the total PEF by separating the total two-body terms. This procedure can be done by separating the pair-interaction function into two parts, which usually consists of two terms; a repulsive term and an attractive term.

The total interaction energy of a system was expressed as the linear combination of two-body functions

$$\Phi = D_{21}\varphi_{21} + D_{22}\varphi_{22} \quad (2.3)$$

where φ_{21} , and φ_{22} are the two-body energies

$$\varphi_{2k} = \sum_{i<j} U_{ij}^{(2k)}, \quad k = 1, 2. \quad (2.4)$$

The general form of the two-body ($U_{ij}^{(2k)}$) atomic interactions was defined in terms of inter-atomic distances as

$$U_{ij}^{(2k)} = A_k r_{ij}^{-\lambda_k} e^{-\alpha_k r_{ij}^2}, \quad k = 1, 2 \quad (2.5)$$

The two-body interaction function contains three parameters (A_k, λ_k, α_k). This form of the pair-potential function does not give a bound state for a dimer. It requires two such functions one for the repulsive branch and one for the attractive branch of a complete pair-potential function. A combination of two such functions form an exact pair-potential function

$$U_{ij} = U_{ij}^{(21)} + U_{ij}^{(22)} \quad (2.6)$$

Therefore there are two sets of parameters for the two-body potential functions, one for the repulsive part (A_1, λ_1, α_1) in $U_{ij}^{(21)}$ and one for the attractive part (A_2, λ_2, α_2) in $U_{ij}^{(22)}$ [45]. These parameters were determined [46] by fitting the exact pair-potential function, Eq. (2.6), to the experimentally determined curve, which are taken from [47]. The profile of pair potential, Eq. (2.6) is given in Figure 2.1.

D_{21} and D_{22} are the linear combination parameters, which contain, in some sense, the contribution of many-body effects. As a whole the present PEF contains eight parameters for a monatomic system. The combination $D_{21}U_{ij}^{(21)} + D_{22}U_{ij}^{(22)}$ may be considered as effective pair-potential, its profile is also given in Fig. 2.1.

The linear parameters (D_{21}, D_{22}) were determined by considering the bulk stability condition, at $T = 0$ K, ($\partial\Phi/\partial V = 0$), and the cohesive energy expression, Eq. (2.3). In Eq. (2.7)

$$0 = D_{21}\varphi'_{21} + D_{22}\varphi'_{22} \quad (2.7)$$

the prime denotes the first derivative with respect to volume, V , which is

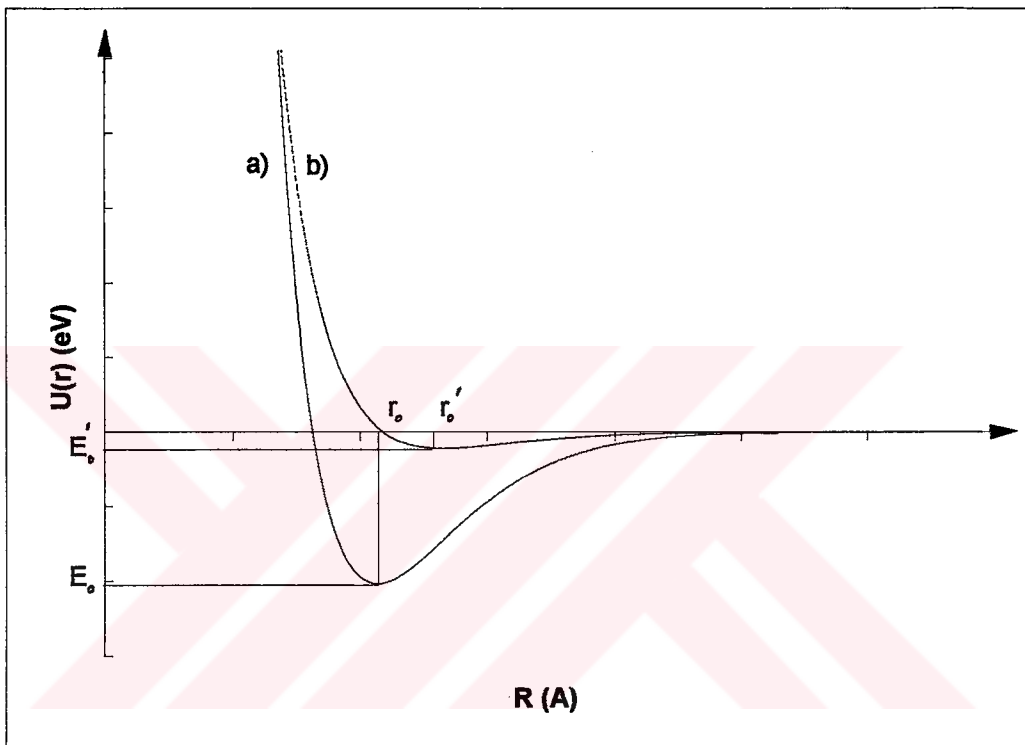


Figure 2.1: The potential profiles of a) pair potential, and b) effective pair potential. $E_0 = -2.035 \text{ eV}$, $E'_0 = -0.22 \text{ eV}$, $r_0 = 2.22 \text{ \AA}$, and $r'_0 = 2.74 \text{ \AA}$.

the atomic volume in the crystal. The PEF satisfies the bulk cohesive energy, and the bulk stability condition exactly. The present PEF, although formed from pair–interactions only, contains many–body effects.

The parameters of the present PEF are given in Table 2.1. This PEF was applied for the stability and energetics of copper microclusters. It also gives the elastic constants and bulk modulus of copper. Therefore the present PEF satisfies some cluster and bulk properties of copper.

Table 2.1: Parameters of the PEF for copper [45]. In the determination of the PEF parameters energy was taken in eV and distance was taken in Å.

Quantity	Value
A_1	110.766008000
λ_1	2.090459460
α_1	0.394142248
A_2	-46.164978300
λ_2	1.498530830
α_2	0.207225507
D_{21}	0.436092895
D_{22}	0.245082238

CHAPTER 3

COMPUTER SIMULATION METHODS

3.1 Historical background

The invention of the electronic computer opened up a new possibility of relating the macroscopic properties of matter to the microscopic information on atoms and molecules. The main idea of computer simulation is as follows. The configurations of a many-particle system are reproduced by numerical computations, and thermodynamical properties are calculated by averaging certain quantities over configurations thus obtained. In the molecular dynamics method, the equations of motion of classical mechanics are integrated numerically and the movement of each particle is followed. In the Monte Carlo method, another typical simulation method, a stochastic process is employed to change the configurations.

3.1.1 Early days

The study of properties of a liquid state has been a challenging problem for computer simulations. Contrary to gas and solid states, there is no simple model to describe well the nature of a liquid state. In a gas state, a noninteracting ideal gas is a good model, and we can learn much about the nature

of a solid from a perfect crystal simulations have been devoted to elucidating the nature of a liquid.

In the 1950s, two basic computer simulation methods, the Monte Carlo [49] and molecular dynamics [50] methods, were introduced. Already at this early stage, many of the basic techniques of computer simulations (periodic boundary conditions, the truncation of the interaction potential, and its correction) were employed.

Alder and Wainwright [50, 51] applied the molecular dynamics method to the study of hard-sphere systems. This is generally considered as the first molecular dynamics simulation. The discovery that a fluid-solid phase change exists even in a hard-sphere system without an attractive force was a surprise. The simulations in these early days were pioneering works in every respect, they had a great impact by the discovery of unexpected results, and confirmed the importance of the numerical approach for the many-body problem.

A system with a continuous interacting potential was investigated by Vineyard *et al.* [52] in a study of the radiation damage of a crystal and by Rahman [53] in a study of a Lennard-Jones liquid. Vineyard's work was the first computer simulation application to the material sciences. Rahman's work was also a milestone; he investigated many dynamical properties in liquids.

Verlet [54] determined a phase diagram of a Lennard-Jones system. In this study, he introduced the so-called Verlet algorithm (the most popular

numerical integration method in the molecular dynamics simulations).

The simulation of liquid water by Rahman and Stillinger [55] marked the start of the 1970s. This also indicated a change of the trend in simulation. The target of study changed from a simple model system to a realistic one. Rahman and Stillinger used an empirical potential for their study of liquid water, but afterwards the interactions between molecules were often determined by the aid of molecular orbital calculations. A typical example is the work by Clementi's group on water-water interactions [56, 57].

Another typical numerical integration method, a predictor-corrector algorithm (Nordsieck and Gear algorithm [58, 59]) is introduced in Rahman and Stillinger's work.

The treatment of the rotation of a rigid body becomes important in the study of molecular systems. The equations of motion for the molecular rotation expressed by using Euler angles have singular points. This is an undesirable feature for numerical integration. Singularity-free algorithms for molecular rotation were introduced by Evans [60] and by Berendsen *et al.* [61]. Evans rewrites the Euler equations for the molecular rotation in terms of quaternions. In this form, the singularities disappear from the equations of motion and it has also the merit that the calculation of the trigonometric functions is not necessary. In the method by Berendsen *et al.*, the equations of motion for an atomic system are solved under the imposition of constraints to fix atomic arrangements in a molecule.

The calculation of the free energy evoked much interest in the 1970s. The

most promising method is an umbrella sampling method [62] based on a weighted average over two different states. A remarkable extension in this line is the method proposed by Frenkel and Ladd [63]. They make possible the direct comparison of the free energy between different crystal structures by gradually replacing the interatomic interactions by an Einstein lattice vibration model.

3.1.2 New methods appeared in the 1980s

The 1980s was a decade of revolution for the molecular dynamics method. Many new algorithms were presented. They may be categorized into the following three groups: (i) simulations in ensembles different from the traditional microcanonical ensemble. This means simulations at constant temperature and pressure. (ii) Nonequilibrium molecular dynamics method, (iii) *Ab initio* molecular dynamics method known as the Car–Parrinello method. These methods are related intrinsically and inspired the development of the methods in different categories.

A common feature of new methods is that they modify the equations of motion in classical mechanics. This modification allowed the adaptation of the computer simulations to various situations [64].

3.2 Simulation in Cluster research

Computer simulation techniques based on atomic considerations provide a useful approach to the study of small clusters. Despite the fact that,

currently, many computer simulation calculations are at a qualitative level, they nevertheless contribute considerably to our understanding of microscopic structures and related processes. Simulation studies not only help scientists to gain proper intuition but, in fact, they are becoming an important tool to aid in the interpretation of many experimental observations. There are three common 'atomic level' computer simulation methods which can be used in small cluster research: molecular dynamics, Monte Carlo and energy minimization.

All three of these simulation methods are based on some type of a potential energy function which describes the total interaction energy among the atoms as a function of their positions in the cluster. In general, finding an appropriate potential energy function constitutes the most important and difficult part of these simulation techniques, which are basically long iterative procedures. Therefore, it is necessary to describe the total potential energy of the system in terms of semi-empirical or model potential functions with simple analytic forms. While for smaller size clusters more complex functions (perhaps even functions based on first principles) can be utilised, in the case of larger clusters the computational time becomes prohibitively long, requiring the use of functions with the simplest possible forms to represent the interactions among the atoms in the cluster. Before discussing these methods it is necessary to define ensembles briefly.

3.3 Ensembles

For molecular dynamics (MD) and Monte Carlo (MC) techniques there are a variety of statistical ensembles that may be employed. Simulations have been reported using the following types:

- The microcanonical ensemble: In which the ensemble contains a constant number of particles (N), constant volume (V) and constant internal energy (E); hence the alternative denotation as the (NVE) ensemble.
- The canonical ensemble: Where (N), (V) and temperature (T) are constant hence the (NVT) ensemble.
- The isothermal–isobaric ensemble: Where pressure (P) is constant, in addition to (N), (T); hence the (NPT) ensemble.
- The grand canonical ensemble: In which the number of particles is not constant but may vary in order to achieve constant chemical potential μ and denoting the ensemble by (μVT) .

MD simulations are most easily carried out in the microcanonical ensemble, while MC is naturally suited to the canonical ensemble. However, much modern MD work is undertaken using constant pressure (NPT) ensemble, while MC simulations using the (μVT) ensemble have been extensively studied.

3.3.1 Canonical-Ensemble Averages

Consider a system of N identical particles, each of mass m , contained in the d -dimensional ‘volume’ V , at temperature T . The restriction to identical particles is made principally for notational convenience and does not, of course, imply any restriction on the MD method. Let particle i have position \mathbf{r}_i and velocity \mathbf{v}_i . It is designated a point in $2dN$ -dimensional phase space by

$$\mathbf{x}^N = [\mathbf{r}^N, \mathbf{v}^N] \quad (3.1)$$

$$\mathbf{r}^N = [\mathbf{r}_1, \mathbf{r}_2, \dots, \mathbf{r}_N], \quad \mathbf{v}^N = [\mathbf{v}_1, \mathbf{v}_2, \dots, \mathbf{v}_N] \quad (3.2)$$

For particles interacting through the potential $U(\mathbf{r}^N)$, the canonical-ensemble probability density in phase space is

$$\rho(\mathbf{x}^N) = Z(N, V, T)^{-1} e^{-\beta H(\mathbf{x}^N)} \quad (3.3)$$

$$H(\mathbf{x}^N) = \frac{1}{2} m \sum_{i=1}^N v_i^2 + U(\mathbf{r}^N) \quad (3.4)$$

$$Z(N, V, T) = \int d\mathbf{x}^N e^{-\beta H(\mathbf{x}^N)} \quad (3.5)$$

$$\beta = 1/kT \quad (3.6)$$

where k is the Boltzmann constant and the phase integral is defined by

$$\int d\mathbf{x}^N \equiv \int_V d\mathbf{r}^N \int d\mathbf{v}^N \quad (3.7)$$

$$\int d\mathbf{r}^N \equiv \int_V d\mathbf{r}_1 \int_V d\mathbf{r}_2 \dots \int_V d\mathbf{r}_N, \quad \int d\mathbf{v}^N \equiv \int d\mathbf{v}_1 \int d\mathbf{v}_2 \dots \int d\mathbf{v}_N \quad (3.8)$$

The velocity integrals can be evaluated explicitly to yield

$$Z(N, V, T) = (2\pi/m\beta)^{dN/2} Q(N, V, T) \quad (3.9)$$

$$Q(N, V, T) = \int_V d\mathbf{r}^N e^{[-\beta U(\mathbf{r}^N)]} \quad (3.10)$$

where $Q(N, V, T)$ is called the configurational integral.

The ensemble average of a phase function $f(\mathbf{x}^N)$ is then

$$\langle f(\mathbf{x}^N) \rangle \equiv \int d(\mathbf{x}^N) \rho(\mathbf{x}^N) f(\mathbf{x}^N) \quad (3.11)$$

which reduces for functions of position to

$$\langle f(\mathbf{r}^N) \rangle = Q(N, V, T)^{-1} \int_V d(\mathbf{r}^N) e^{[-\beta U(\mathbf{r}^N)]} f(\mathbf{r}^N) \quad (3.12)$$

The equilibrium thermodynamic functions of the system follow from the Helmholtz energy $A(N, V, T)$,

$$e^{[-\beta A(N, V, T)]} = (m/h)^{dN} (N!)^{-1} Z(N, V, T) = \lambda^{-dN} (N!)^{-1} Q(N, V, T) \quad (3.13)$$

$$\lambda = (\beta h^2 / 2\pi m)^{1/2} \quad (3.14)$$

where h is Planck's constant. For particles interacting through the pairwise-additive potential $u(r_{ij})$,

$$U(\mathbf{r}^N) = \sum_{i < j} u(r_{ij}) \quad (3.15)$$

where,

$$\sum_{i < j} \equiv \sum_{i=1}^{N-1} \sum_{j=i+1}^N, \quad r_{ij} = |\mathbf{r}_i - \mathbf{r}_j| \quad (3.16)$$

one obtains the internal energy

$$E(N, V, T) = (\partial[\beta A] / \partial \beta)_{N, V} = \frac{1}{2} dN kT + \langle U(\mathbf{r}^N) \rangle \quad (3.17)$$

and the pressure

$$p = -(\partial A / \partial V)_{N,T}$$

$$pV/NkT = 1 - 2\beta \langle W(\mathbf{r}^N) \rangle / dN \quad (3.18)$$

$$W(\mathbf{r}^N) = \frac{1}{2} \sum_{i < j} r_{ij} du(r_{ij}) / dr_{ij} \quad (3.19)$$

The function W is the virial and Eq. (3.18) is the so-called virial equation of state .

The Monte Carlo method is the principal numerical method for the evaluation of expressions of the form Eq. (3.12), as typified by the averages appearing in Eq. (3.17) and Eq. (3.18)[65].

3.4 Molecular Dynamics (MD)

In the molecular dynamics technique the classical equation of motion is solved numerically for a collection of N atoms which constitute the cluster. With the knowledge of the interatomic potentials, the forces acting on the particles may be calculated. The simulation then proceeds by solving Newton's equations for the ensemble by allowing it to evolve through a succession of time steps, each of Δt . In the limit of an infinitely small value of Δt , we can write for the coordinates x_i and velocities v_i of the i^{th} particle before and after Δt :

$$x_i(t + \Delta t) = x_i(t) + v_i(t)\Delta t \quad (3.20)$$

$$v_i(t + \Delta t) = v_i(t) + \frac{f_i(t)}{m_i} \Delta t \quad (3.21)$$

where f_i is the force acting on the particle and m_i its mass. In practice a finite value of Δt is, of course used (typically in the range $10^{-15} - 10^{-14}$ sec, details of determining Δt is given in Appendix D) and more sophisticated updating algorithms are employed higher powers of Δt . Depending on the potential energy function used and the type of the system to be simulated, a variety of numerical algorithms is available for this purpose [65, 66, 67, 68, 69] ([67] is advised especially for non-equilibrium molecular dynamics algorithms (NEMD)). The method generates a time-order series of atomic coordinates representing the motion of every atom in the system. Kinetic energies are incorporated with the calculation scheme, therefore temperature effects are intrinsically included in the result. In principle, molecular dynamics calculations with a sufficient number of iterations can simulate any time-dependent (non-equilibrium), as well as equilibrium, quantity. Using velocities of particles evaluated in every step, one can obtain the velocity autocorrelation function from which the frequency distribution spectrum for the microcluster can be calculated.

3.4.1 Molecular Dynamics Averages

While the calculation of the properties of matter by ensemble methods has attained pre-eminence in statistical mechanics, nevertheless the method of time averages along a dynamical trajectory is no less fundamental a technique to determine such properties. It is defined that the molecular dynamics

average of a phase function $f(\mathbf{x}^N)$ as

$$\bar{f} = \lim_{t \rightarrow \infty} \bar{f}(t), \quad \bar{f}(t) = \frac{1}{t} \int_0^t dt' f[\mathbf{x}^N(t')] \quad (3.22)$$

Here $\mathbf{x}^N(t)$ denotes the phase space trajectory determined by the classical equations of motion

$$\frac{d\mathbf{r}_i}{dt} = \mathbf{v}_i, \quad \frac{d\mathbf{v}_i}{dt} = -\frac{1}{m} \frac{\partial}{\partial \mathbf{r}_i} U(\mathbf{r}^N) \quad (3.23)$$

together with certain boundary conditions and initial data $\mathbf{x}^N(0) \equiv \mathbf{x}^N$.

While dynamical methods can evidently have application beyond the field of equilibrium averages, for the most part we shall be concerned with the latter. The relationship between ensemble averages and time averages then introduces the field of ergodic theory.

The quasi-ergodic hypothesis asserts the equivalence of the MD time average Eq. (3.22) with an ensemble average in an ensemble characterized by the constants of the dynamical motion, the volume V , the number of particles N , and at least for most numerical applications, the energy $H(\mathbf{x}^N)$. The existence of other constants of motion depends on the boundary conditions; for periodic boundary conditions, linear momentum

$$\mathbf{M}(\mathbf{v}^N) = m \sum_{i=1}^N \mathbf{v}_i \quad (3.24)$$

is also conserved. We refer to an ensemble characterized by specified values of N , V , energy E , and linear momentum \mathbf{M} as the ‘molecular dynamics ensemble’ and write averages therein as [65]

$$\langle f(\mathbf{x}^N) \rangle_{NVEM} = \int d\mathbf{x}^N \rho_{NVEM}(\mathbf{x}^N) f(\mathbf{x}^N) \quad (3.25)$$

$$\rho_{NVE\mathbf{M}}(\mathbf{x}^N) = Z(N, V, E, \mathbf{M})^{-1} \Delta(\mathbf{x}^N; E, \mathbf{M}) \quad (3.26)$$

$$\Delta(\mathbf{x}^N; E, \mathbf{M}) = \delta[E - H(\mathbf{x}^N)] \delta[\mathbf{M} - \mathbf{M}(\mathbf{v}^N)] \quad (3.27)$$

$$Z(N, V, E, \mathbf{M}) = \int d\mathbf{x}^N \Delta(\mathbf{x}^N; E, \mathbf{M}) \quad (3.28)$$

where the δ function for a d -vector argument \mathbf{y} is defined by

$$\delta(\mathbf{y}) = \prod_{j=1}^d \delta(y_j) \quad (3.29)$$

3.4.2 Approach to Equilibrium

As noted above, the molecular dynamics ensemble is characterized by fixed values of N , V , E and \mathbf{M} . All states \mathbf{x}^N consistent with these values are equiprobable. According to the quasi-ergodic hypothesis, the trajectory $\mathbf{x}^N(t)$ starting from \mathbf{x}^N should, except possibly for a set of initial phases of zero measure, spend equal amounts of time in regions of allowed phase space having equal measure. Nevertheless there exist exceptional states \mathbf{x}^N for which the short-time behaviour of $\mathbf{x}^N(t)$ is unusual in that the phase function $f(\mathbf{x}^N)$ corresponding to a macroscopic observable departs from its ensemble average significantly. In Fig. 3.1 it is illustrated such a situation by a sketch of $\Delta f(t) = f[\mathbf{x}^N(t)] - \langle f(\mathbf{x}^N) \rangle_{NVE\mathbf{M}}$. The initially large values of Δf tend to decrease with time until the fluctuations become of order $1/N$, with only rare fluctuations of larger magnitude.

An example of such an initial state is provided by the situation in which the particles in one-half of V have much higher energy than those in the other half, at least if N is of macroscopic magnitude. Other such exceptional

states will not necessarily appear so unusual. Nevertheless we speak of the system as non-equilibrium initially, as approaching equilibrium when Δf is large and decreasing, and as in equilibrium at subsequent times, when Δf is of order $1/N$. While large fluctuations should reappear after the Poincaré recurrence time, this time is enormous for fluid systems, at least if N is not too small [65].

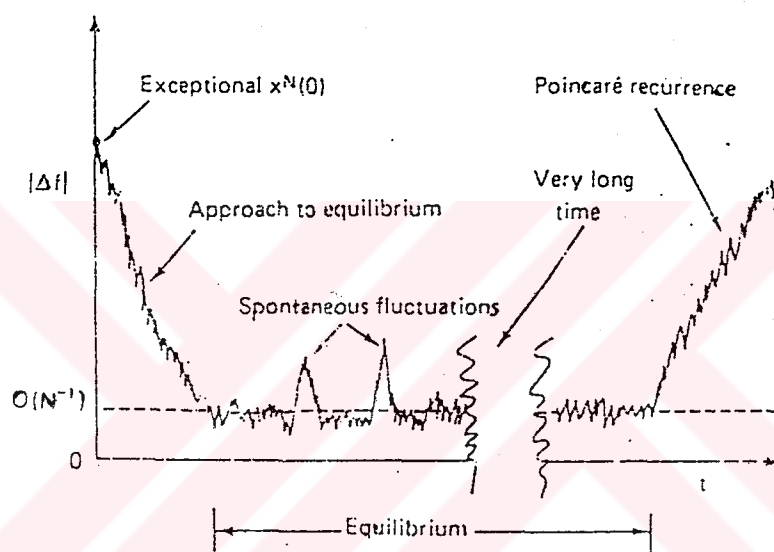


Figure 3.1: Time evolution of a dynamical system.

3.4.3 Time-Saving Techniques

The careful selection of an interaction algorithm is not the only means of conserving computer resources in molecular dynamics. In this section two devices will be discussed so that a significant amount of computer time

during the generation of a phase space trajectory can be saved: equilibration on subsystems and bookkeeping.

At the beginning of a molecular dynamics calculation, one must normally assign initial conditions, that is, the values of the position and velocity for each particle in the system. There are a number of ways of doing this: the molecules may be arranged on a lattice, a configuration from another molecular dynamics calculation may be modified to satisfy the new density condition, or a random configuration may be generated using a Monte Carlo technique. The velocities may be assigned from a Maxwell-Boltzmann distribution at the desired temperature by a rejection technique (see Appendix B), or they may even all be assigned an initial value of zero. In any case, the initial state selected will in general not be an 'equilibrium state' consistent with the desired temperature and density. As a result, the temperature (which is found from the sum of squares of the molecular velocities) will be seen to drift away from its initial value as the integration proceeds. When this happens, the integration must be halted and the velocities multiplied by a scale factor to restore the temperature to its desired value (see Appendix C). This procedure is then repeated until equilibrium is achieved, that is, until the temperature drift is replaced by fluctuations about the desired value.

In some molecular dynamics work, the process of equilibration has accounted for a substantial fraction of the total computer time devoted to the calculation. If the intermolecular potential has a sufficiently short range,

however, it is possible to use only a fraction of the molecular dynamics system for equilibration. One can set aside a subsystem containing, say, an n of the total number of molecules, select initial conditions, and allow the subsystem to come to equilibrium. After equilibrium has been reached, the subsystem is replicated n -fold in space to generate the full system. All of the velocities are reassigned from a Maxwell-Boltzmann distribution, and equilibration is resumed. After the replication, equilibrium for the full system is usually established quickly. Since the integration for the subsystem is fast compared to the full system, this equilibration procedure results in a significant saving of computer time.

It can be identified at least two problems arising in the initialization and equilibration procedures which have been mentioned above. One problem concerns the relaxation time of the system. The basic time step h determines the real time of the simulation. If the intrinsic relaxation time is long, many steps are required in order for the system to reach equilibrium. For some systems the number of time steps may be prohibitively large for the present speed of computers. However, it is possible in some circumstances to circumvent the difficulty by an appropriate scaling of the variables. Examples of where this is possible are systems near second-order transitions.

In connection with the relaxation time one has to face the possibility that the system is trapped in a metastable state. Long-lived metastable states may not show an appreciable drift in the kinetic or potential energy. Especially for systems investigated near two-phase coexistence, say between

liquid and gas, this danger arises.

The second problem is that the system might have been set up in an irrelevant part of the phase space. This problem can be handled by performing simulations with initial conditions and different lengths.

Bookkeeping procedures take advantage of the finite range of the intermolecular potential. At any given time during a molecular dynamics calculation, most pairs of molecules are separated by a distance much greater than the effective range of intermolecular potential r_t . It makes little sense then to calculate the distance between each pair of molecules at each time step of the integration. In the 'standard' method of bookkeeping, one imagines a sphere of radius slightly larger than r_t centered at each molecule. A list is then kept in computer storage of all the other molecules that are within each molecule's sphere. Of course, if molecule j is listed in molecule i 's sphere, it should not be necessary to list molecule i explicitly in molecule j 's sphere. Then when the total force and torque exerted on molecule i are to be calculated, only these neighbors needed be considered. The list of neighbors must, of course, be updated periodically. In sufficiently dense fluids this is done approximately every ten integration steps. The difference between the radius of the bookkeeping sphere and r_t must be larger than the maximum distance a molecule might reasonably travel in these ten steps, at the given temperature of the system. This method consequently requires that after each ten steps the list of particles within the bookkeeping sphere of each particle must be updated, a procedure requiring the calculation of the distance

between every distinct pair of molecules, of which there are $N(N - 1)/2$. For an N -molecule system, the computer time required for this updating is roughly proportional to N^2 .

In an alternative bookkeeping scheme, the molecular dynamics box is divided into a number of small cells. At the beginning of each time step, the particular molecules in each cell are listed. The cells are then scanned, and relative distances are calculated only for pairs of molecules in neighboring cells. In this method the time required at each step is always proportional to N . Thus, as the number of particles in the system increases, this method should become faster than the previous bookkeeping method.

One of the important parameters in this form of bookkeeping is the size v (volume) of the cell. There is a trade off between the cycle time and accuracy. This procedure only includes interactions between the particles in nearest-neighbor cells. If $v^{1/3}$ is less than or equal to the interaction range, then important interactions will be missed. On the other hand, if v is large so that on the average a large fraction of the N particles occupy each cell, the procedure becomes an inefficient as if no bookkeeping were used.

The use of bookkeeping procedures will in general yield dramatic reduction in the consumption of computer time in molecular dynamics and can therefore greatly increase the scope of such calculations [68, 69].

3.5 Monte Carlo (MC)

MC is a technique of computational statistical mechanics ideally suited for

calculating ensemble averages in the canonical (NVT) ensemble. The simulation proceeds via the generation of successive configurations of the ensemble by a series of random moves each of which normally involves the displacements of only one particle. Once a sufficient number (normally several thousand) configurations have been generated, ensemble averages are straightforwardly calculated.

Possibly the most crucial technical feature of an MC simulation concerns the 'acceptance' procedure, i.e. the criteria used to decide whether a configuration generated after a move should be included in the final set of configurations which are stored and used in calculating ensemble averages. Monte Carlo techniques employed in small-cluster simulations are, in general, based on the Metropolis procedure [49, 70, 71, 72], the method in effect weights the probability of acceptance of a new configuration by its Boltzmann factor. Starting from an initial configuration, atoms in the cluster are randomly displaced according to the Maxwell-Boltzmann distribution. At thermal equilibrium, the probability that an assembly of atoms will achieve the energy ΔE required to transform from one particular equilibrium configuration to another is given by the Boltzmann factor $\exp(-\Delta E/kT)$. A new 'trial' position is sampled at random for the atom, within a small spherical region about its current position, and the change in energy associated with movement to this trial position is computed. A random number is then selected from the interval (0, 1) and compared with the Boltzmann factor for the trial move. If the random number is smaller than the Boltzmann factor the move is made;

otherwise the atom is retained at its original position. After generation of a sufficient number of Monte Carlo steps (ensuring that the phase space is sampled ergodically) the desired quantities are calculated as ensemble averages from position-dependent quantities estimated in every step. By this method any equilibrium quantity can be calculated as a function of temperature which is introduced via the Maxwell-Boltzmann factor. In grand canonical (μVT) MC a move may involve the inclusion of an additional particle in the ensemble.

MC has similar computational requirements to MD and like MD, MC calculations normally have an equilibration period followed by a production run. But unlike MD, the successive configurations in the simulation have no relationship on time. MC is therefore inherently more restricted than MD as time dependent phenomena cannot be directly investigated. However, the method is the simplest and most direct way of understanding simulations in the canonical and grand-canonical ensembles. Moreover, it continues to have considerable vitality with important fundamental developments.

3.6 Energy minimization (EM)

EM methods are restricted to the prediction of static structures and of these properties which can be described within an harmonic (or quasi-harmonic) dynamical approximation; there is no explicit inclusion of atomic motions. The static method is based on a simple minimization technique to find the configuration of a cluster corresponding to the nearest energy minimum. It

is a temperature-independent approach and can be regarded as the $T = 0$ K case. Despite these limitations, the methods have proved to be powerful and remarkably flexible in their range of applications. The basis of the method is; the energy $E(x)$ is calculated, using knowledge of interatomic potentials, as a function of all the structural variables, x , (e.g. atomic coordinates or bond lengths and angles); an initial configuration is specified and the variables are adjusted, using an iterative computational method, until the minimum energy configuration is obtained, i.e. the system runs 'down-hill' as shown diagrammatically in Figure 3.2. The method may be extended if vibrational properties of the energy minimum are calculated using the harmonic approximation; thus for a molecule normal coordinate analysis may be used, while for a solid, standard lattice dynamical methods are employed. This allows entropies in addition to enthalpies to be calculated and hence 'free-energy' minimization may be performed.

The most important technical features of energy minimization methods concern first the type of summation procedures used in evaluating the total interaction energy; this problem is, however, common to all atomic simulations. Secondly the choice of the computational minimization method.

The simplest methods employ the energy function alone and search over configuration space until the minimum is located. While such methods may be suitable for very simple problems with few variables, they are unacceptably inefficient in almost all contemporary studies. Much greater efficiency is obtained using gradient techniques in which the first derivatives $\partial E/\partial x_i$ with

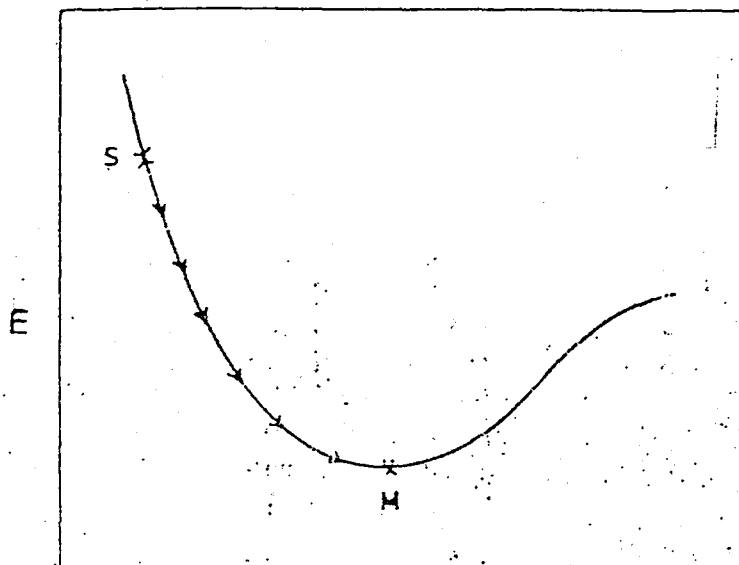


Figure 3.2: Energy (E) minimization with respect to some structural variable x . The system runs down from the starting point S to the minimum M.

respect to all the structural variables x_i are calculated. These then guide the direction of minimization.

EM techniques have the advantage of simplicity and versatility which has led to them being widely applied to e.g. crystal structure modelling (of both organic and inorganic materials), to studies of the conformation of molecules, including biological macromolecules (note that in these fields, EM is often referred to be the term 'molecular mechanics') and to modelling of defects in solids. Compared with many other computer simulation techniques EM requires little CPU time, and this factor allows the use of more complex and sophisticated potentials.

Nevertheless EM methods are severely limited; they inherently omit any representation of atomic motions and time dependent phenomena. Moreover,

even given the usefulness of the static approximation, there is a major additional difficulty in that EM techniques can only be guaranteed to locate the nearest local minimum to the starting point of the calculation as shown diagrammatically in Figure 3.3. The local minimum problem may be very severe as in studies of protein conformations, although less difficulties are encountered in solid state applications. There is no general solution to the problem. The use of several starting points in a calculation is obviously advisable.

In addition, energy minimized configurations may be input into dynamical simulations (using the techniques summarized below) which may allow energy barriers to be surmounted. There remains, however, no guarantee that the lowest energy or global minimum has been located. Depending upon the initial configuration chosen, however, this method can provide only one of the many configurational energy levels associated with the cluster. Even for clusters in smaller size regimes, finding the cluster configuration corresponding to the lowest energy level (the ground state) may turn out to be a quite difficult job, particularly if the gross structure of the symmetry group of the ground state cannot be guessed initially. In order to increase the probability of finding the global minimum, a rather large number of initial guesses must be made and, even then, minima located in narrow catchment regions may easily be missed.

On the other hand, if one uses physical intuition, usually as a set of growth rules deduced from the behaviour of macroscopic systems, to generate configurations which are likely to lead to the global minimum, the general

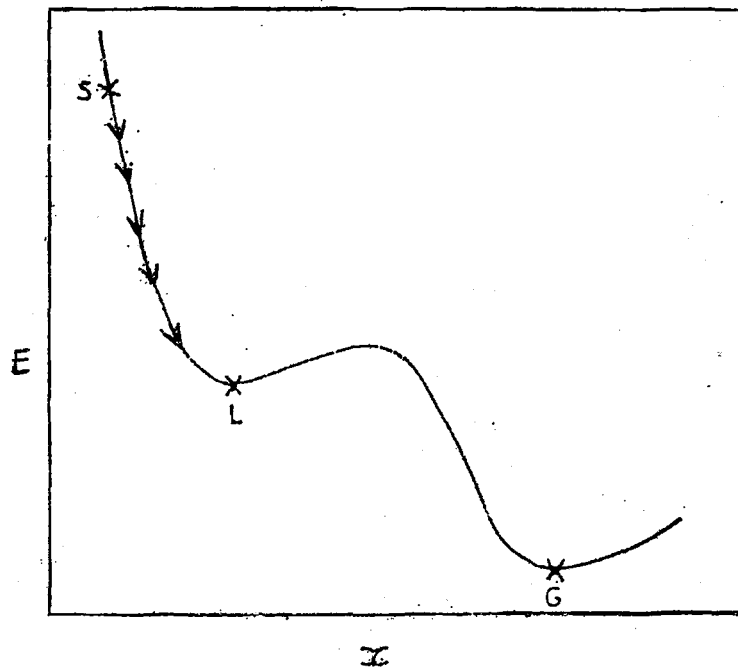


Figure 3.3: Illustration of the local minimum problem with the system running from S to the local minimum L, despite the presence of lower global minimum G.

tendency is to miss low-symmetry solutions [73].

EM remains, however, a widely used technique, which is of considerable value provided its limitations are borne in mind. It is undoubtedly most appropriate as a 'refinement technique' for improving structural models based on approximate knowledge from experiment and from other sources. By the same way force minimization method is also commonly used in most of the static models.

CHAPTER 4

CALCULATIONS & RESULTS

4.1 Shell-like Copper Clusters

In the first part of this work, we studied the structural stability and energetics of isolated small Copper clusters, Cu_n ($n = 13, 19, 43, 55, 79, 87$) and medium size cluster ($n = 135$) at temperatures $T = 1 K$ and $T = 300 K$ by using Molecular-Dynamics technique. Clusters are generated from fcc crystal structure such that: an atom was taken at the center and first nearest-neighbour distance (d_{nn}) as the radius of the first shell, then the second nearest-neighbour distance as the radius of the second shell, and so on up to 7 shells. The number of atoms contained with respect to shells is given in Table 4.1.

We relaxed these clusters by using Erkoç potential which is explained in the second chapter. The total interaction energy has been calculated for each cluster. The graphs of Potential Energy versus Molecular-Dynamics steps (MD) for each cluster at $T = 1 K$ and $T = 300 K$ are given in Figs. 4.1–4.7, respectively. It is seen that the clusters with $n = 19, 79,$ and 87 at

Table 4.1: Total number of atoms in the cluster with respect to shell size.

Shell Number (N_s)	Number of Atoms
1	13
2	19
3	43
4	55
5	79
6	87
7	135

$T = 1 K$, and $n = 19, 79$, and 87 at $T = 300 K$ reach equilibrium quickly; on the other hand, the clusters with $n = 13, 43, 55$, and 135 at $T = 1 K$, and $n = 13, 43, 55$, and 135 at $T = 300 K$ reach equilibrium relatively longer time because of the presence of a lower minima.

The radial distribution functions for each cluster were calculated by taking the atoms around the central atom into account. The graphs of Radial Distribution Function vs Distance for each cluster at Ideal, $T = 1 K$ and $T = 300 K$ are given in Figs. 4.8–4.14. Initial radii $r_n (\equiv d_{nn})$ of fcc spherical clusters and calculated average radii $r_i, i = 1 - 7$, are given in Tables 4.2–4.3 at $T = 1 K$ and $T = 300 K$, respectively. In the $n = 135$ cluster the atoms in the 5th and 6th shells mixed after relaxation, in this situation r_5 looks larger than r_6 ; this artifact is due to keeping the initial labels of atoms till the end of the calculation. The present results shows that there is expansion of shells

after MD relaxation except $n = 135$ cluster. For microclusters, there is a relation such as; $r_0 < r < d_{nn}$ where r_0 is the dimer separation, d_{nn} is the nearest-neighbour distance in the crystal and r is the cluster value. We have found that the order changes for shell-like clusters. The analogy is such that; $r_0 < d_{nn} < r$. In addition to this expansion, there exist some distortions in the cluster structures. Cluster structures were given in Figs. 4.15–4.21 for Ideal, at $T = 1 K$ and at $T = 300 K$ cases, respectively, from top to bottom.

The average interaction energy per atom, Φ/n , for each cluster is calculated. The calculated values for Ideal, $T = 1 K$ and $T = 300 K$ are given in Table 4.4. By ideal case, it is meant the potential energy configuration with the initial, crystalline like coordinates. By $T = 1 K$ and $T = 300 K$ cases it is meant the final step potential energy configuration of the system approaching the equilibrium after MD relaxation. The variation of average interaction energy per atom, $E_b = \Phi/n$, as a function of the cluster size is plotted in Fig. 4.22. It has been found that the average interaction energy per atom in the cluster decreases and reaches an asymptotic value as cluster size increases. There is an exponential-like decay for Cu_n ($n = 13, 19, 43, 55, 79, 135$). The behaviour is different for $n = 87$ cluster: slope gets positive value; the number ($n = 87$) corresponding this cluster may be considered as a "magic number". The decay is fast for $n = 13, 19, 43$ and small for $n = 55, 79, 135$ clusters.

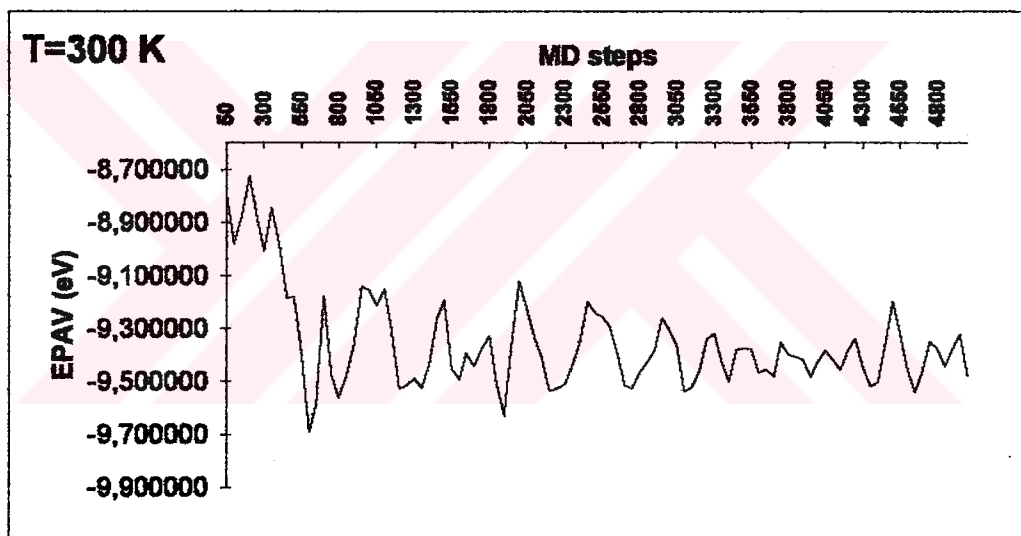
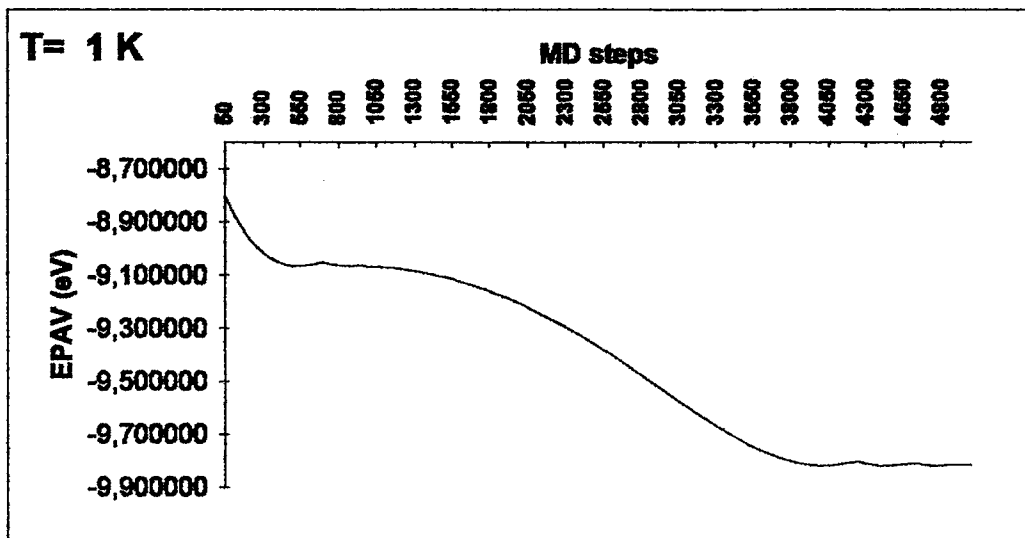


Figure 4.1: Potential Energy (in eV) vs MD steps for $n = 13$ cluster at $T = 1 K$ and $T = 300 K$.

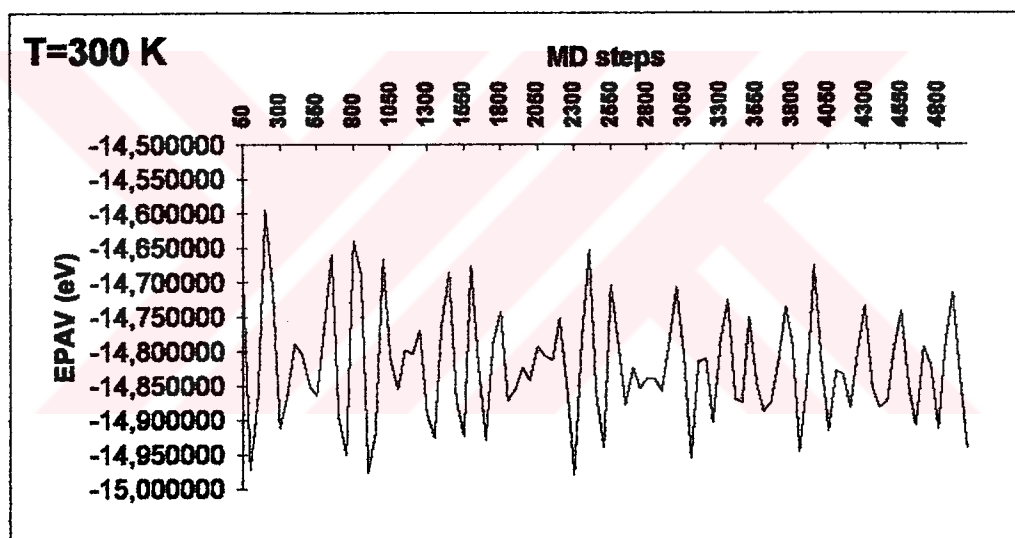
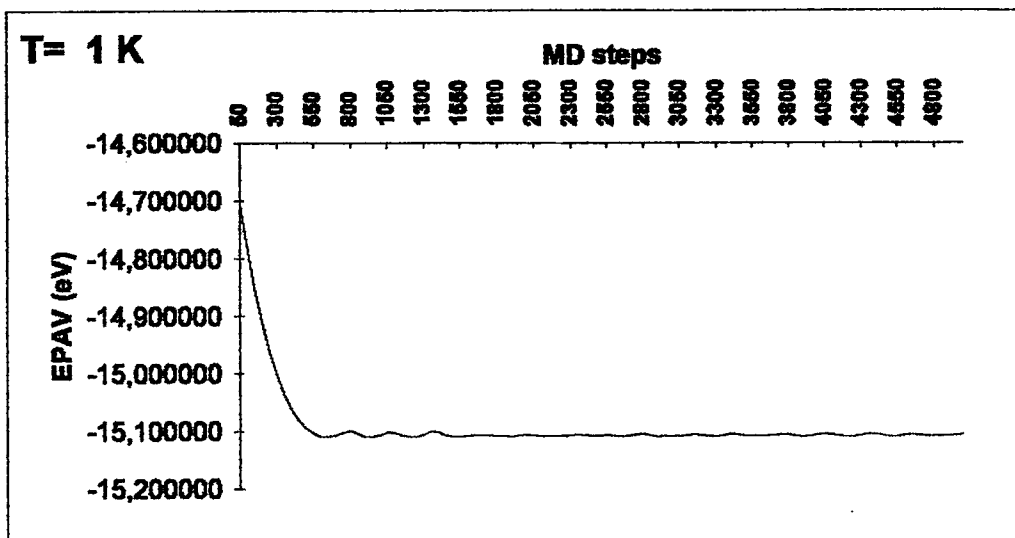


Figure 4.2: Potential Energy (in eV) vs MD steps for $n = 19$ cluster at $T = 1 K$ and $T = 300 K$.

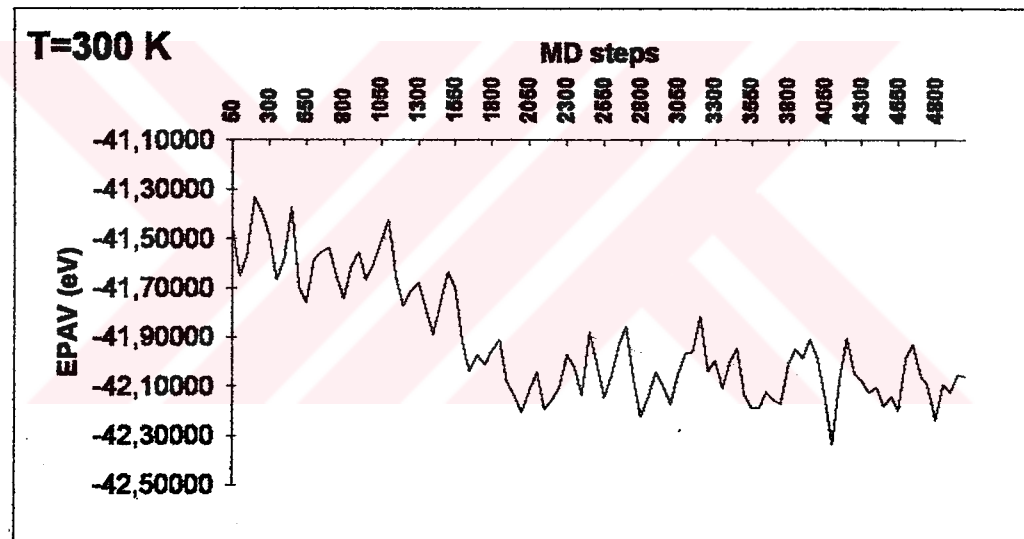
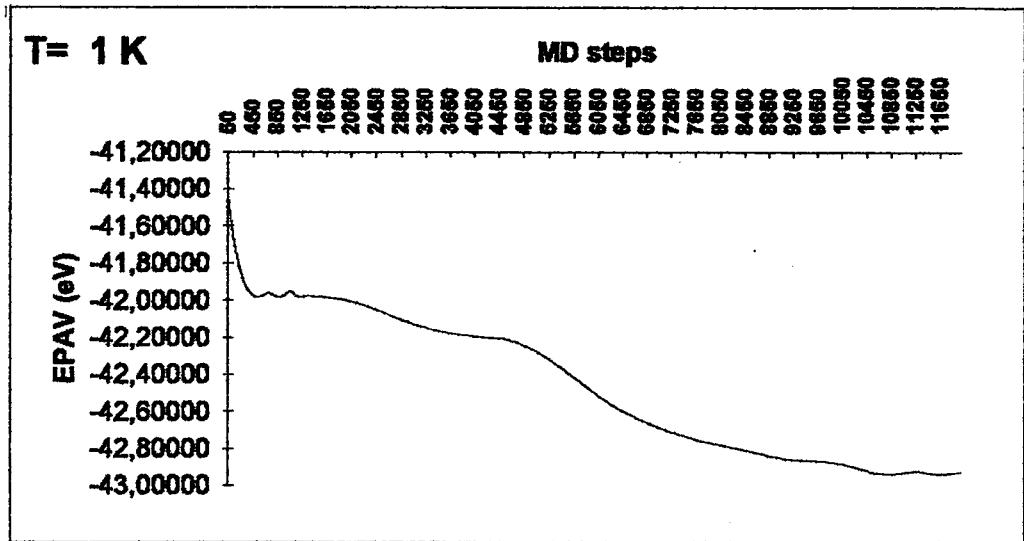


Figure 4.3: Potential Energy (in eV) vs MD steps for $n = 43$ cluster at $T = 1 K$ and $T = 300 K$.

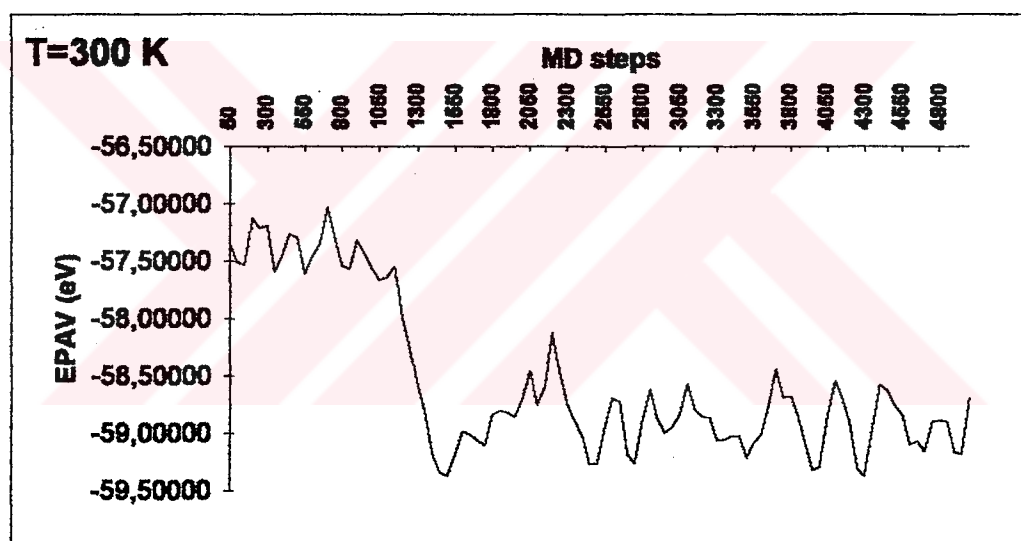
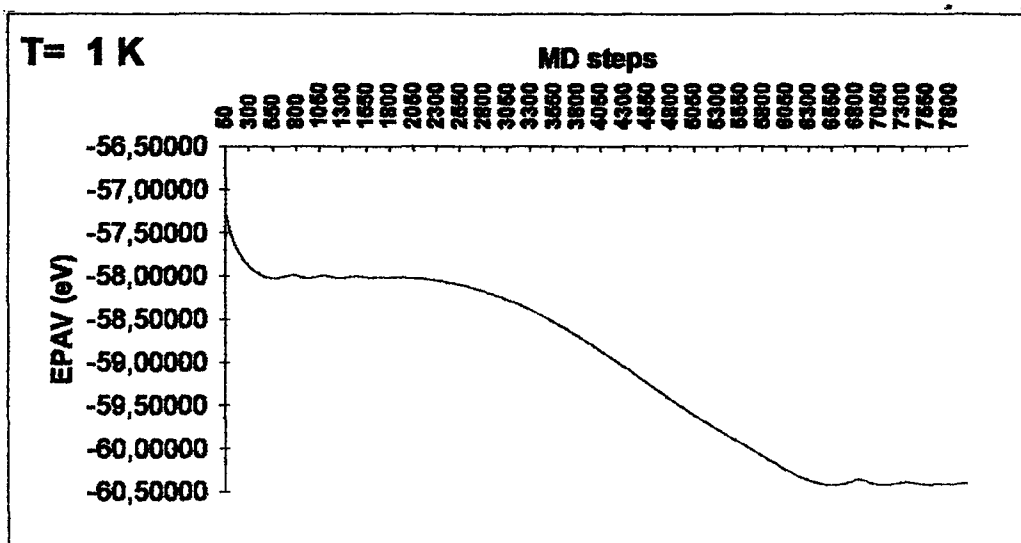


Figure 4.4: Potential Energy (in eV) vs MD steps for $n = 55$ cluster at $T = 1 K$ and $T = 300 K$.

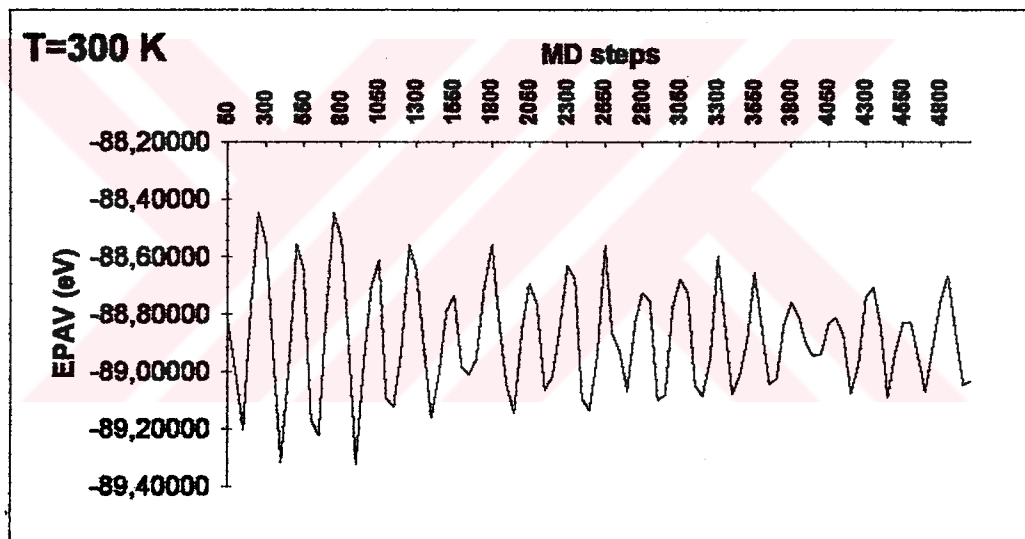
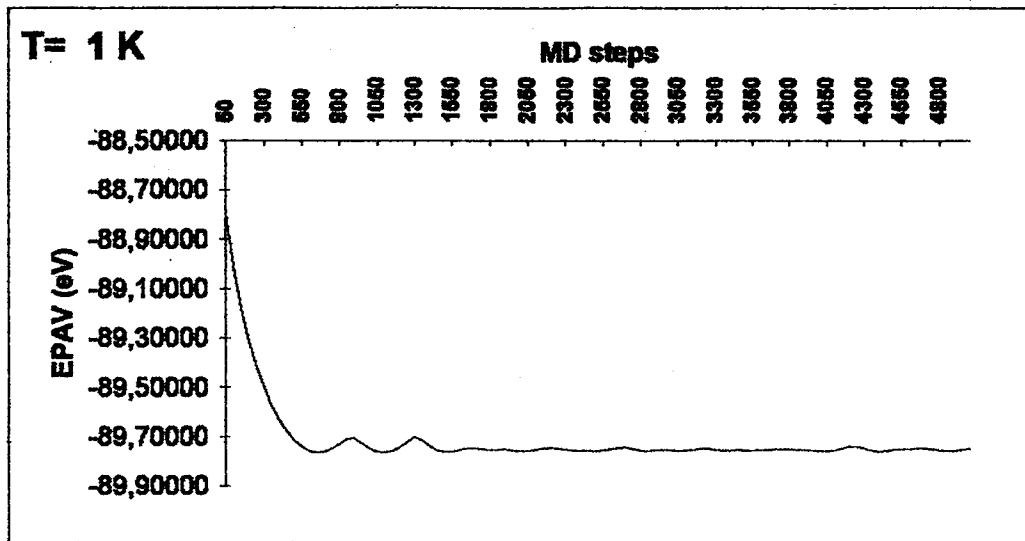


Figure 4.5: Potential Energy (in eV) vs MD steps for $n = 79$ cluster at $T = 1 K$ and $T = 300 K$.

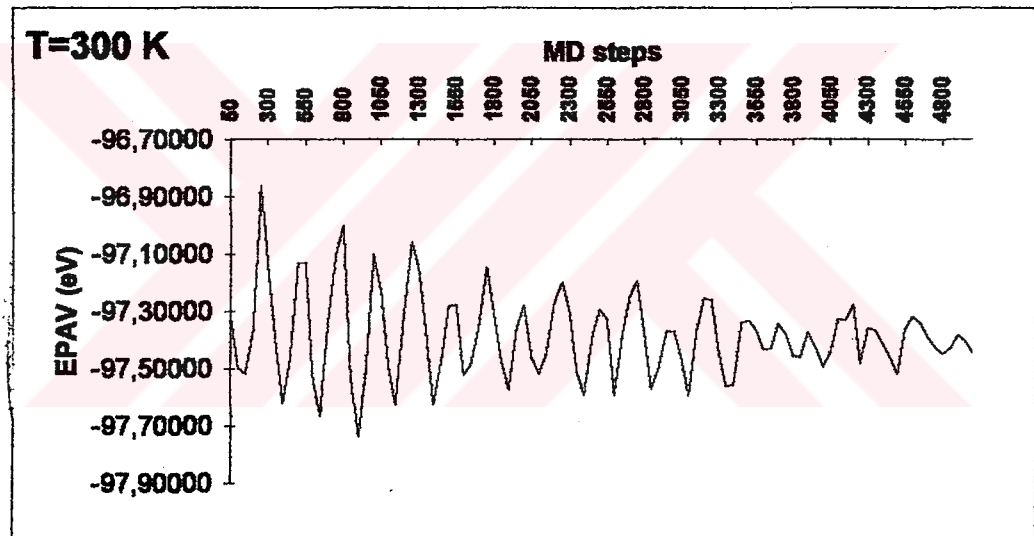
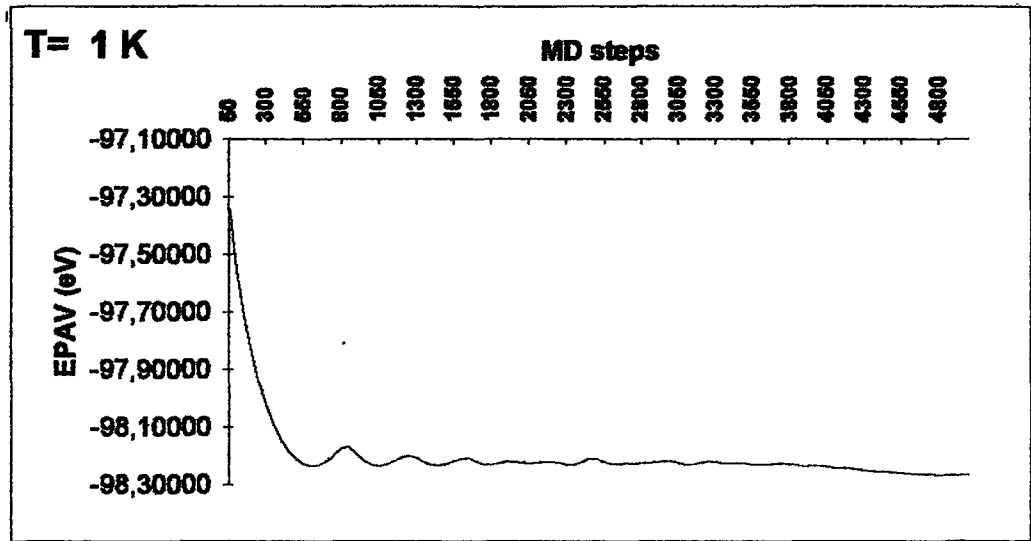


Figure 4.6: Potential Energy (in eV) vs MD steps for $n = 87$ cluster at $T = 1 K$ and $T = 300 K$.

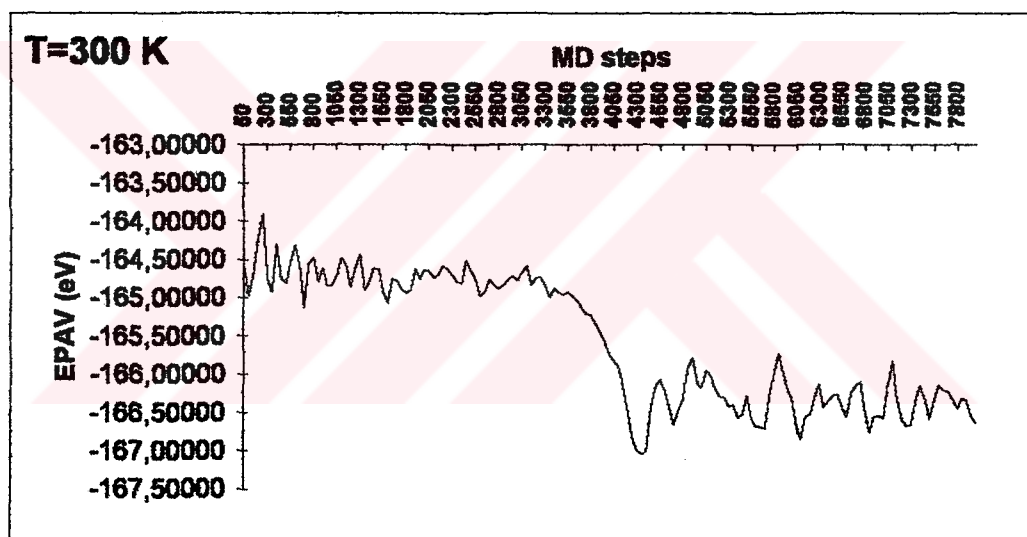
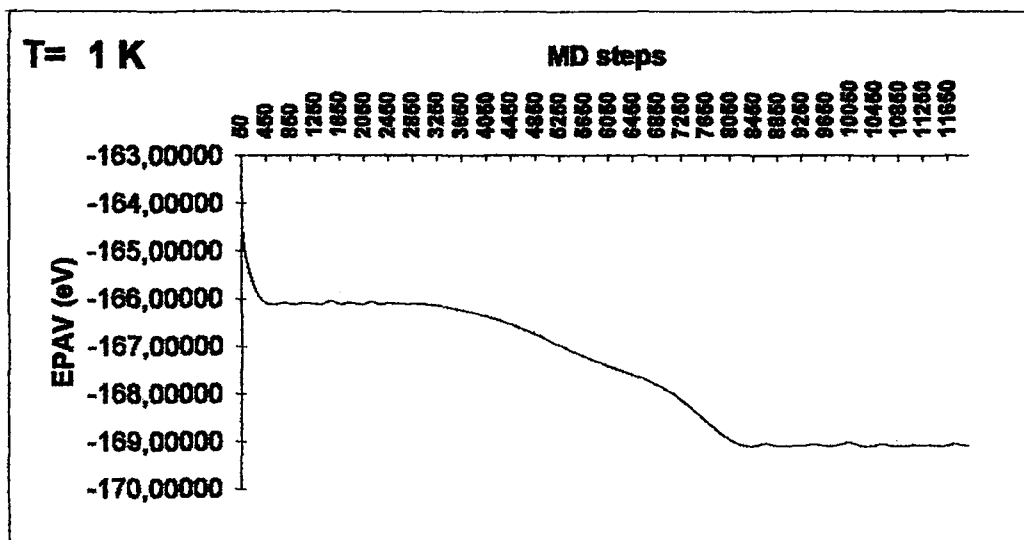


Figure 4.7: Potential Energy (in eV) vs MD steps for $n = 135$ cluster at $T = 1 K$ and $T = 300 K$.

Table 4.2: Initial radius d_{nn} of fcc spherical clusters and calculated average radii (in Å) $r_1, r_2, r_3, r_4, r_5, r_6$ and r_7 at $T = 1$ K.

n	d_{nn}	r_1	r_2	r_3	r_4	r_5	r_6	r_7
13	2.5600	2.6135						
19	3.6204	2.6589	3.8001					
43	4.4341	2.5849	3.8008	4.5026				
55	5.1200	2.4694	4.2979	4.3498	5.1225			
79	5.7243	2.5837	3.6451	4.5068	5.2455	5.8792		
87	6.2707	2.5613	3.6692	4.4518	5.2401	5.9002	6.2945	
135	6.7731	2.4331	4.1508	4.2593	4.9520	6.2784	6.1026	6.6464

Table 4.3: Initial radius d_{nn} of fcc spherical clusters and calculated average radii (in Å) $r_1, r_2, r_3, r_4, r_5, r_6$ and r_7 at $T = 300$ K.

n	d_{nn}	r_1	r_2	r_3	r_4	r_5	r_6	r_7
13	2.5600	2.6344						
19	3.6204	2.6094	3.7727					
43	4.4341	2.6259	3.8886	4.5424				
55	5.1200	2.5103	4.2156	4.4211	5.1836			
79	5.7243	2.5591	3.6366	4.4744	5.2061	5.8446		
87	6.2707	2.5601	3.6712	4.4528	5.2889	5.9095	6.3262	
135	6.7731	2.4463	4.2451	4.2469	4.9518	6.3987	6.0769	6.6166

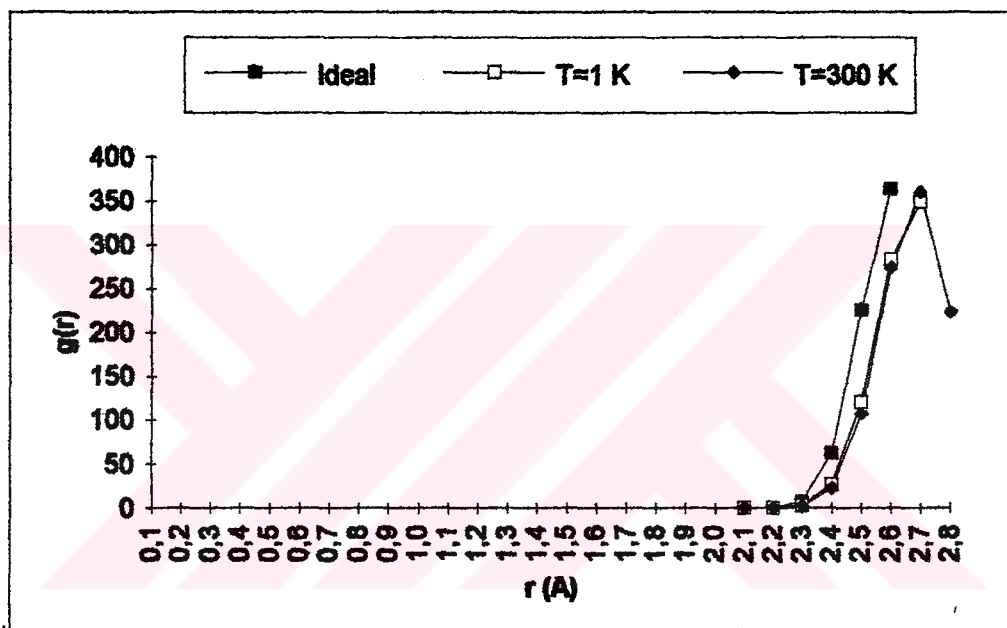


Figure 4.8: Radial Distribution Function vs Distance (in Å) for $n = 13$ cluster at Ideal, $T = 1 K$ and $T = 300 K$.

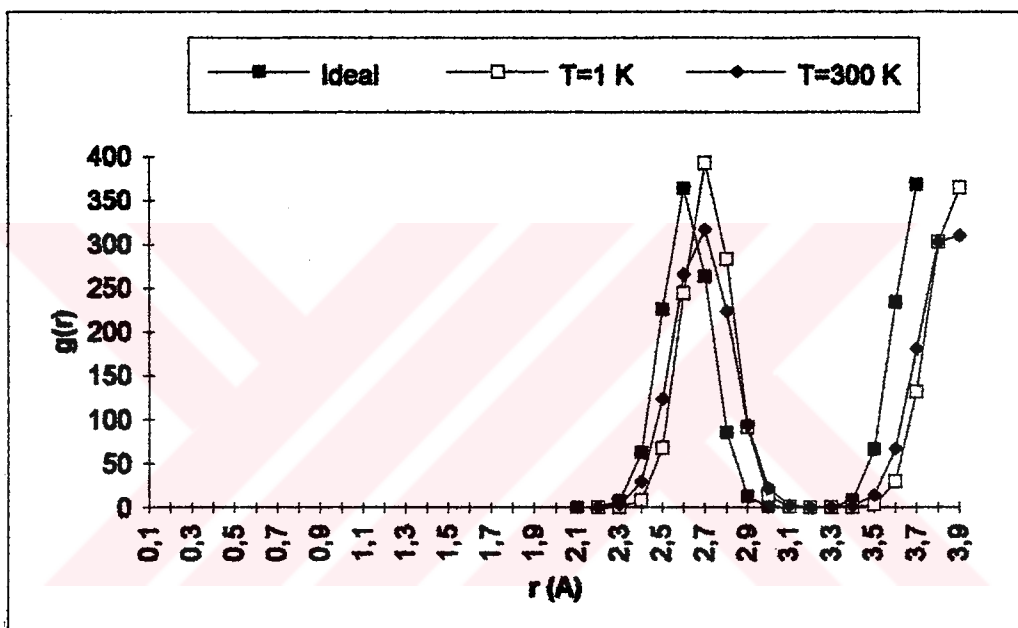


Figure 4.9: Radial Distribution Function vs Distance (in \AA) for $n = 19$ cluster at Ideal, $T = 1 \text{ K}$ and $T = 300 \text{ K}$.

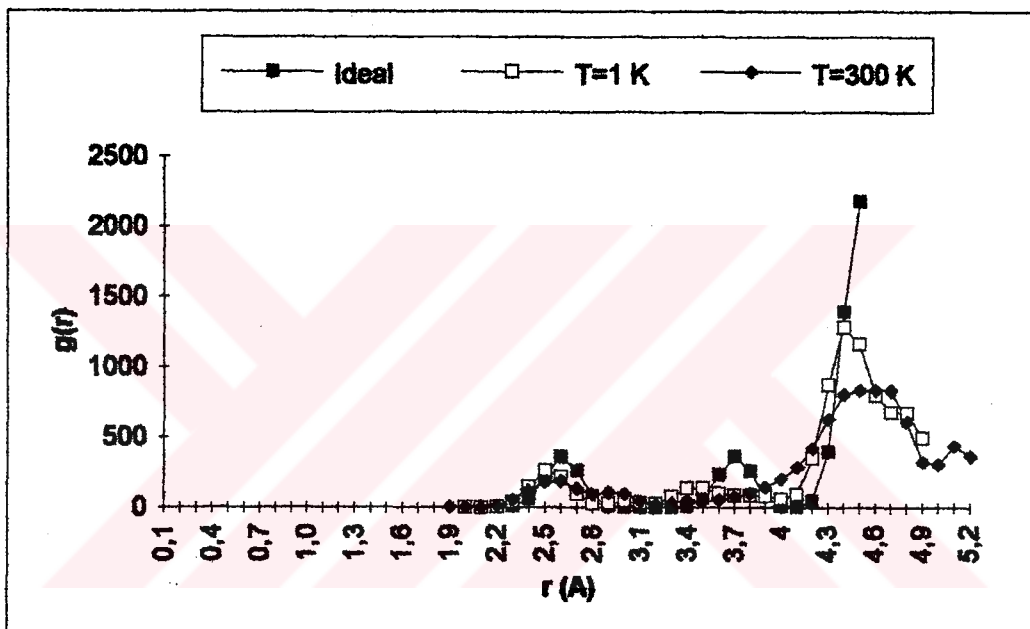


Figure 4.10: Radial Distribution Function vs Distance (in Å) for $n = 43$ cluster at Ideal, $T = 1 K$ and $T = 300 K$.

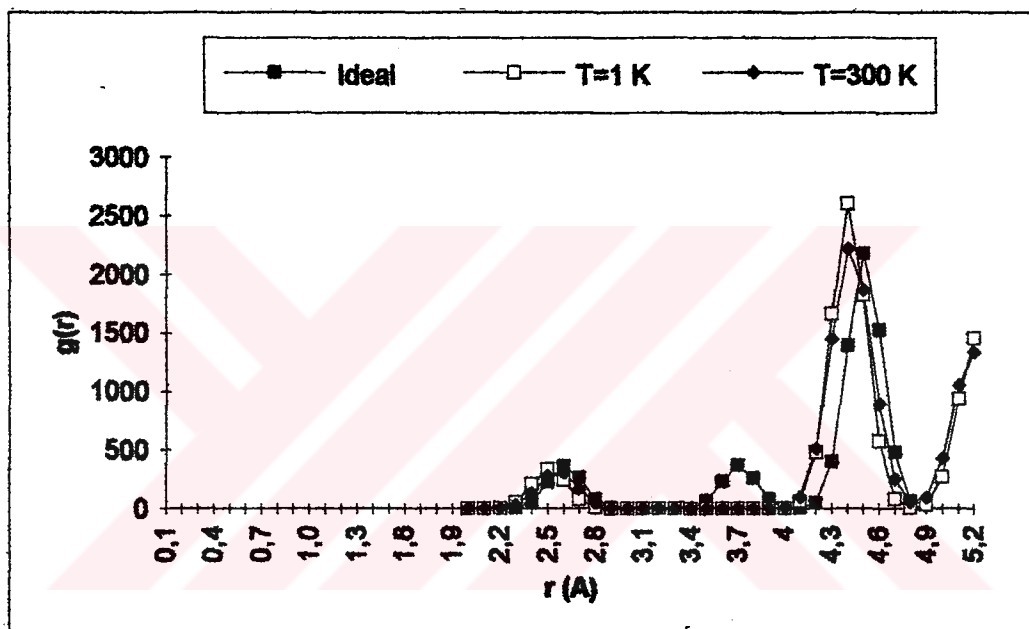


Figure 4.11: Radial Distribution Function vs Distance (in Å) for $n = 55$ cluster at Ideal, $T = 1$ K and $T = 300$ K.

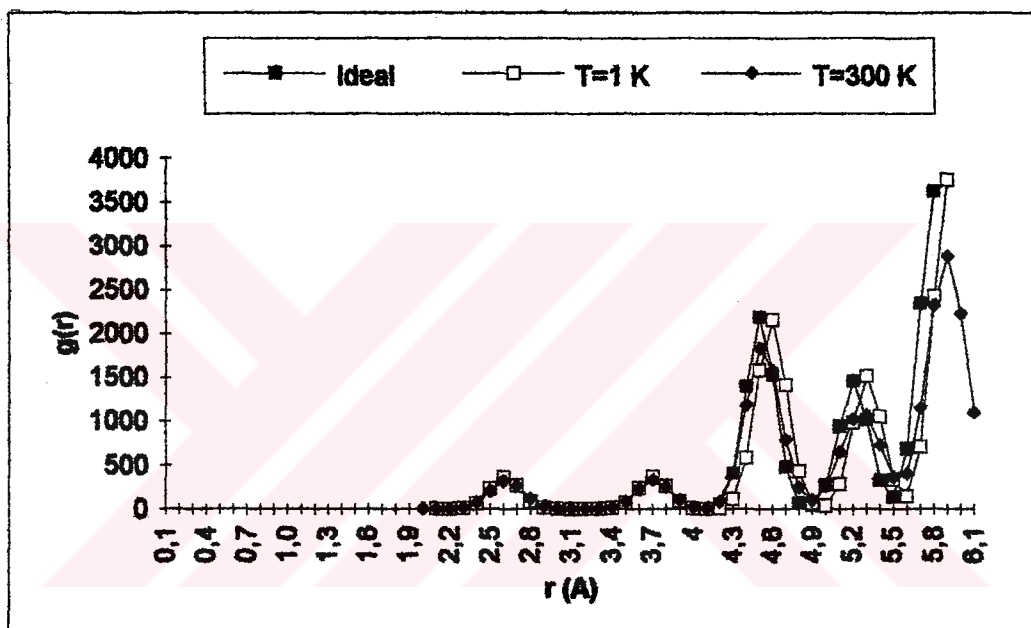


Figure 4.12: Radial Distribution Function vs Distance (in Å) for $n = 79$ cluster at Ideal, $T = 1 K$ and $T = 300 K$.

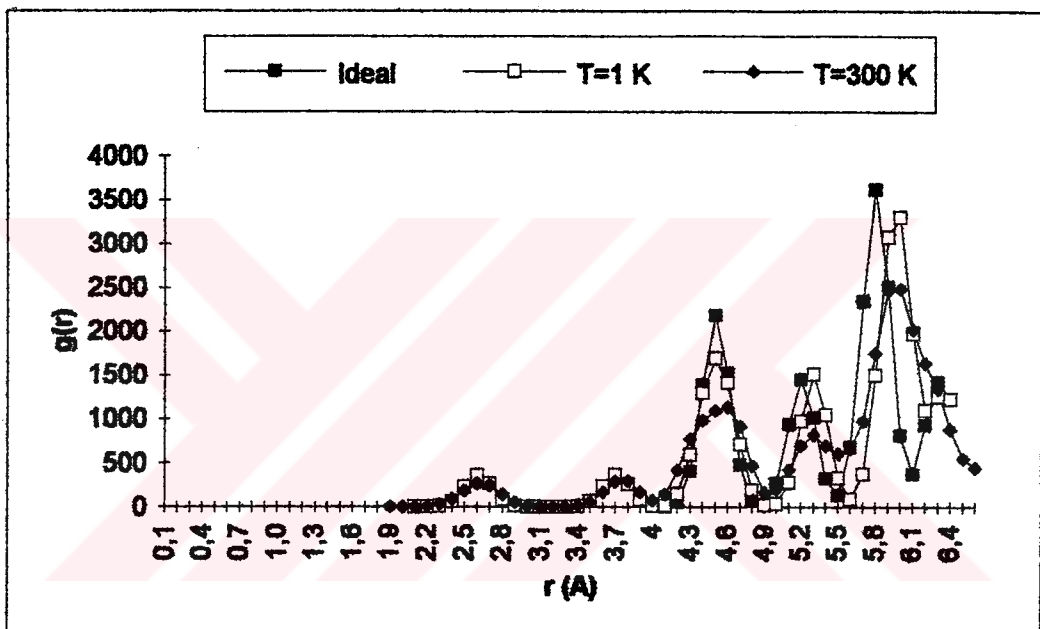


Figure 4.13: Radial Distribution Function vs Distance (in Å) for $n = 87$ cluster at Ideal, $T = 1 K$ and $T = 300 K$.

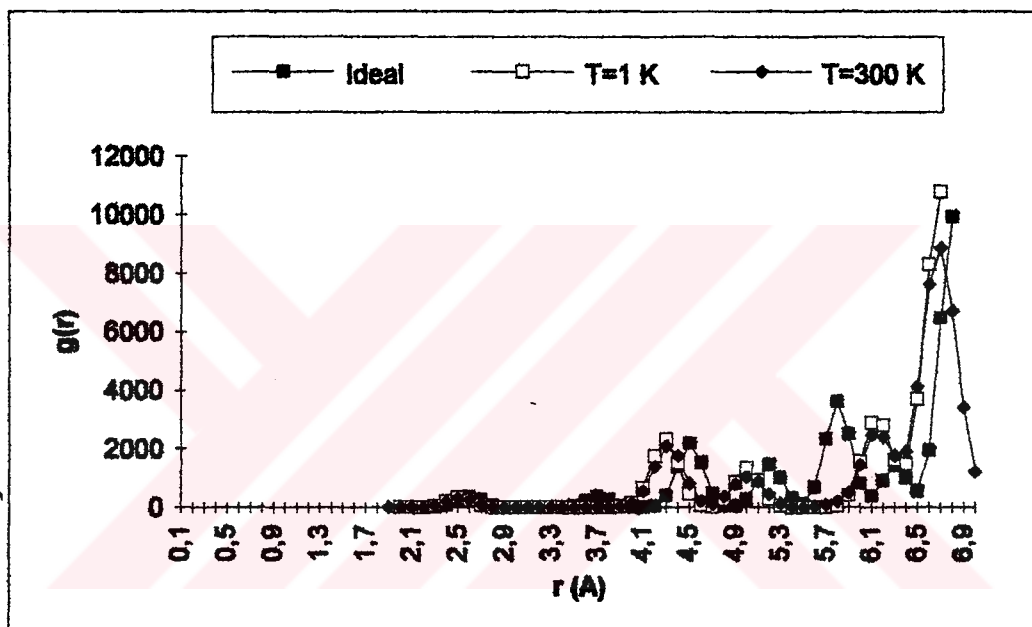


Figure 4.14: Radial Distribution Function vs Distance (in Å) for $n = 135$ cluster at Ideal, $T = 1$ K and $T = 300$ K.

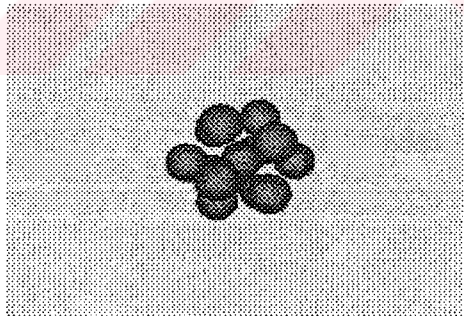
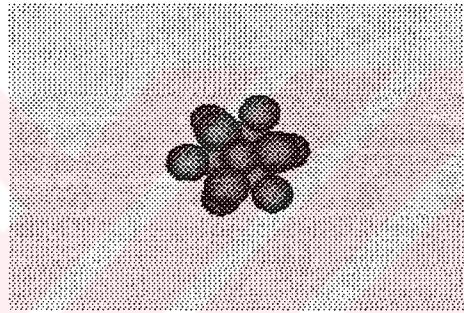
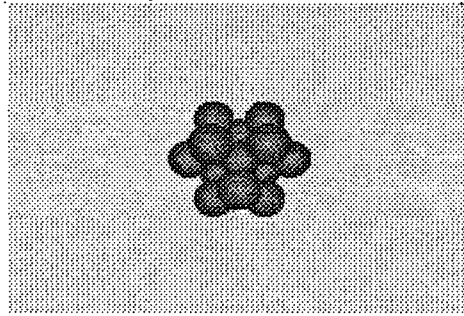


Figure 4.15: Structures for $n = 13$ cluster at Ideal, $T = 1 K$ and $T = 300 K$.

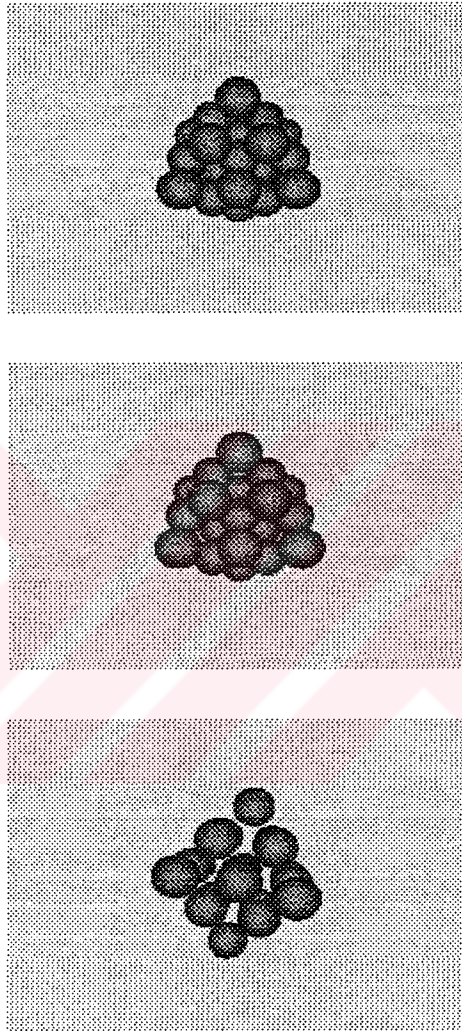


Figure 4.16: Structures for $n = 19$ cluster at Ideal, $T = 1 K$ and $T = 300 K$.

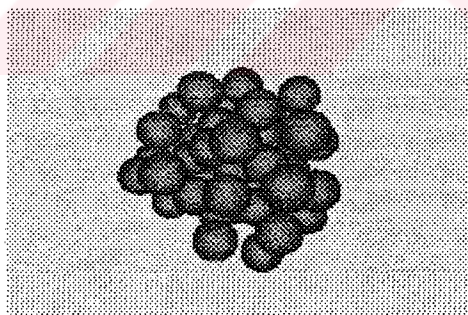
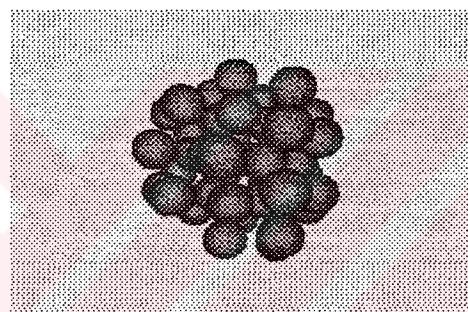
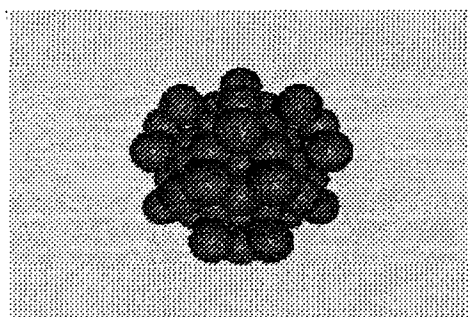


Figure 4.17: Structures for $n = 43$ cluster at Ideal, $T = 1\text{ K}$ and $T = 300\text{ K}$.

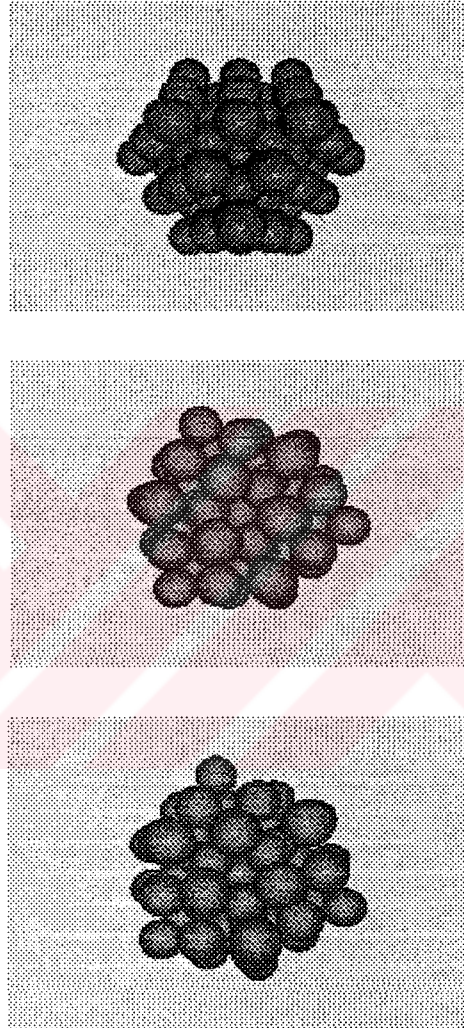


Figure 4.18: Structures for $n = 55$ cluster at Ideal, $T = 1 K$ and $T = 300 K$.

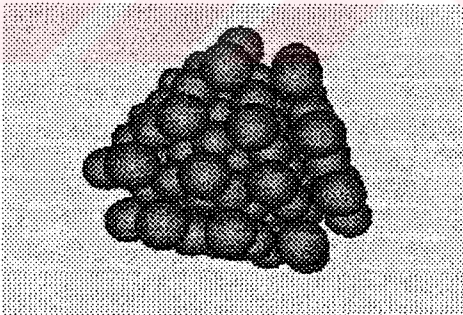
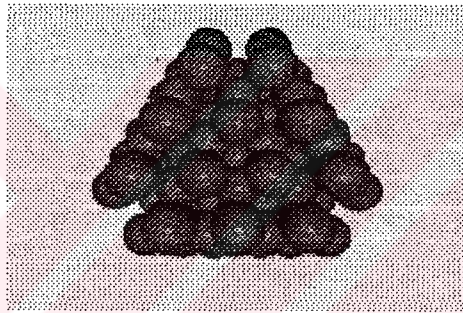
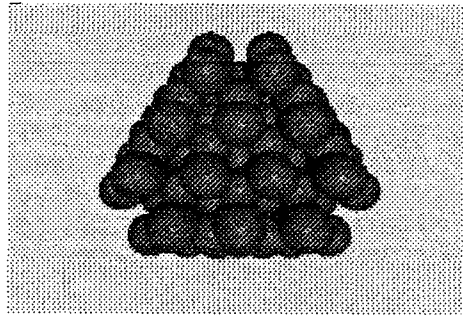


Figure 4.19: Structures for $n = 79$ cluster at Ideal, $T = 1 K$ and $T = 300 K$.

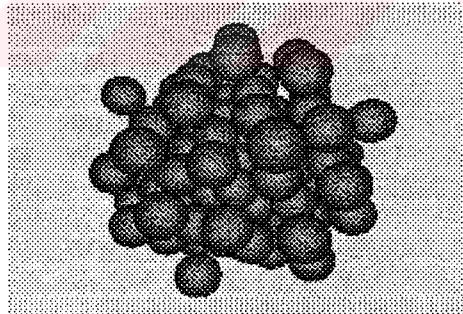
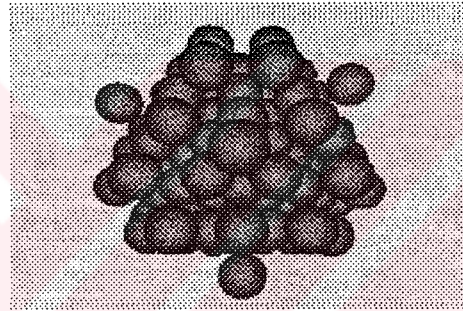
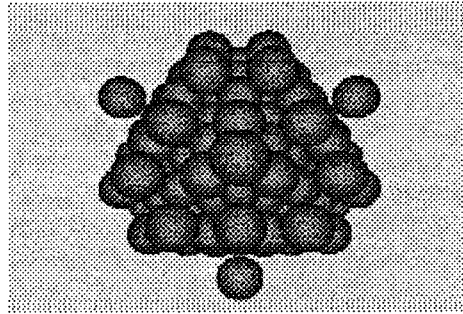


Figure 4.20: Structures for $n = 87$ cluster at Ideal, $T = 1 K$ and $T = 300 K$.

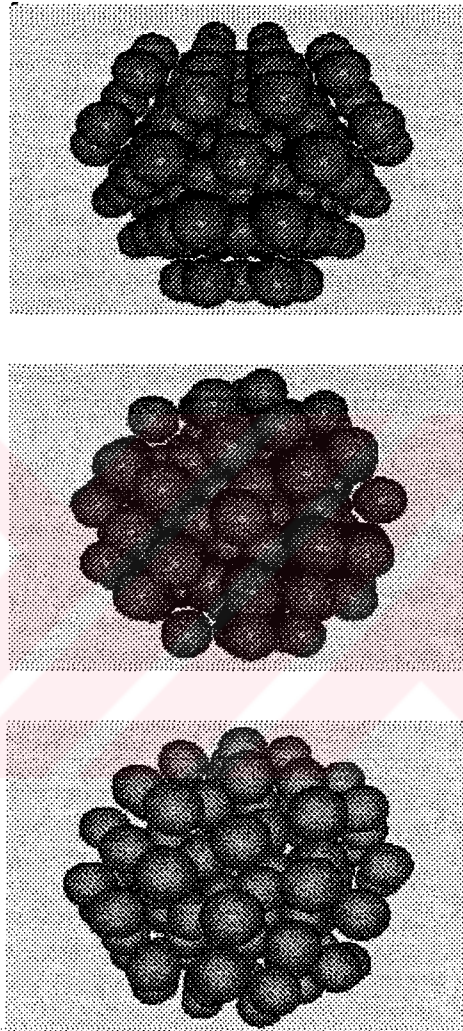


Figure 4.21: Structures for $n = 135$ cluster at Ideal, $T = 1 K$ and $T = 300 K$.

Table 4.4: The average interaction energy per atom (in eV), Φ/n , in Cu_n clusters for Ideal and at $T = 1 K$, $T = 300 K$.

n	Φ/n	Φ/n	Φ/n
	Ideal	at $T = 1 K$	at $T = 300 K$
13	-0.6751	-0.7551	-0.7318
19	-0.7716	-0.7951	-0.7847
43	-0.9621	-0.9949	-0.9785
55	-1.0396	-1.0983	-1.0651
79	-1.1226	-1.1361	-1.1257
87	-1.1174	-1.1295	-1.1203
135	-1.2164	-1.2514	-1.2353

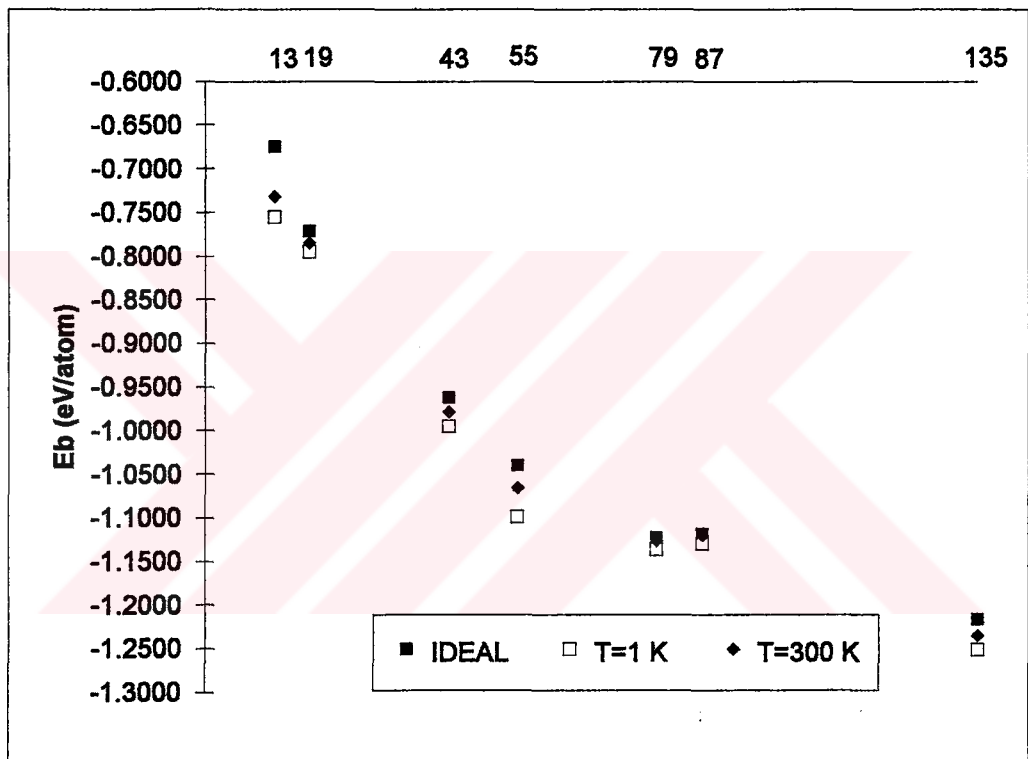


Figure 4.22: The variation of average interaction energy per atom, $\bar{\Phi}=\bar{\Phi}/n$, as a function of the cluster size.

4.2 Melting of Copper Clusters

We have melted $n = 13, 55$ clusters as the second part of our work. We chose $n = 13$ cluster because of its high symmetry, and $n = 55$ cluster to see the melting behaviour of a multi-shell structure. Two models are used for melting of $n = 13$ cluster; first model can be defined as the sequential model while second model as initial configuration model. We started for both model with relaxation at $T = 1$ K. Then using the equilibrium final step coordinates, the system is relaxed by increasing the temperature to $T = 300$ K. After reaching equilibrium at $T = 300$ K, we increased the temperature to $T = 600$ K and relaxed the system with final step coordinates of $T = 300$ K relaxation. We increased the temperature up to $T = 9900$ K by incrementation of 300 K and relaxed $n = 13$ cluster in a sequentially manner for *model1*. However, for *model2* we again increased the temperature up to $T = 9900$ K by incrementation of 300 K but relaxed the system by using only final step coordinates of $T = 1$ K relaxation for all temperatures. The variation of average interaction energy, E_b (in eV), as a function of the temperature (K) for $n = 13$ cluster is plotted for both *model1* and *model2* in Figs. 4.23–4.24, respectively. The present results show that for *model2* the behaviour of the graph is almost straight line and the slope is constant in average manner. There exist distortions and disintegrations but not completely, it is not accurate and consistent with so high temperature. For *model1*, there exists a complete disintegration, and it starts between

$T = 4200 - 4500 \text{ K}$. We have decided with the presence of these results that the melting as a continuous process is described by *modell*. $n = 55$ cluster is melted by using *modell* up to $T = 6900 \text{ K}$. The disintegration starts at $T = 6600 - 6900 \text{ K}$. The variation of average interaction energy, E_b (in eV), as a function of the temperature (K) for $n = 55$ cluster is plotted for *modell* in Fig. 4.25. The distortions in cluster structures between Ideal and starting temperature of disintegration for *modell* is given in Figs. 4.26–4.27 and Figs. 4.28–4.29 for $n = 13$ and $n = 55$, respectively. In the Figs. 4.26–4.27 the dark color atom represents the central atom, and in the Figs. 4.28–4.29 different colored atoms represents different shells. We took the fluctuations of standard deviations of interatomic distances between the central atom and atoms surrounding it as the definition of melting[76]. The graphs of Standard Deviation (σ) versus Temperature (in K) are given in Figs. 4.30–4.31 for $n = 13$ and $n = 55$, respectively. The general trend in the variation of σ with respect to temperature is that σ gradually increases with temperature. However, there are some regions where fluctuations appear in σ . The rapid change in σ describes the beginning of distortion in the structure. It first decreases to a minimum, then increases to a maximum. This shows a high distortions in the structure. This behaviour is considered as melting in clusters. We took the average of the first minimum and the first maximum as the melting temperature. The corresponding values for $n = 13$ and $n = 55$ clusters are $T = 1350 \text{ K}$ and $T = 975 \text{ K}$, respectively. We also studied the standard deviation behaviours of inner shells of $n = 55$

cluster as a function of temperature. The graphs of Standard Deviations of N_s , $s = 1 - 3$ of $n = 55$ versus Temperature are given in Figs. 4.32–4.34. The calculated melting points are given in Table 4.5. The present results show that melting starts from outermost shell for multi-shell clusters.



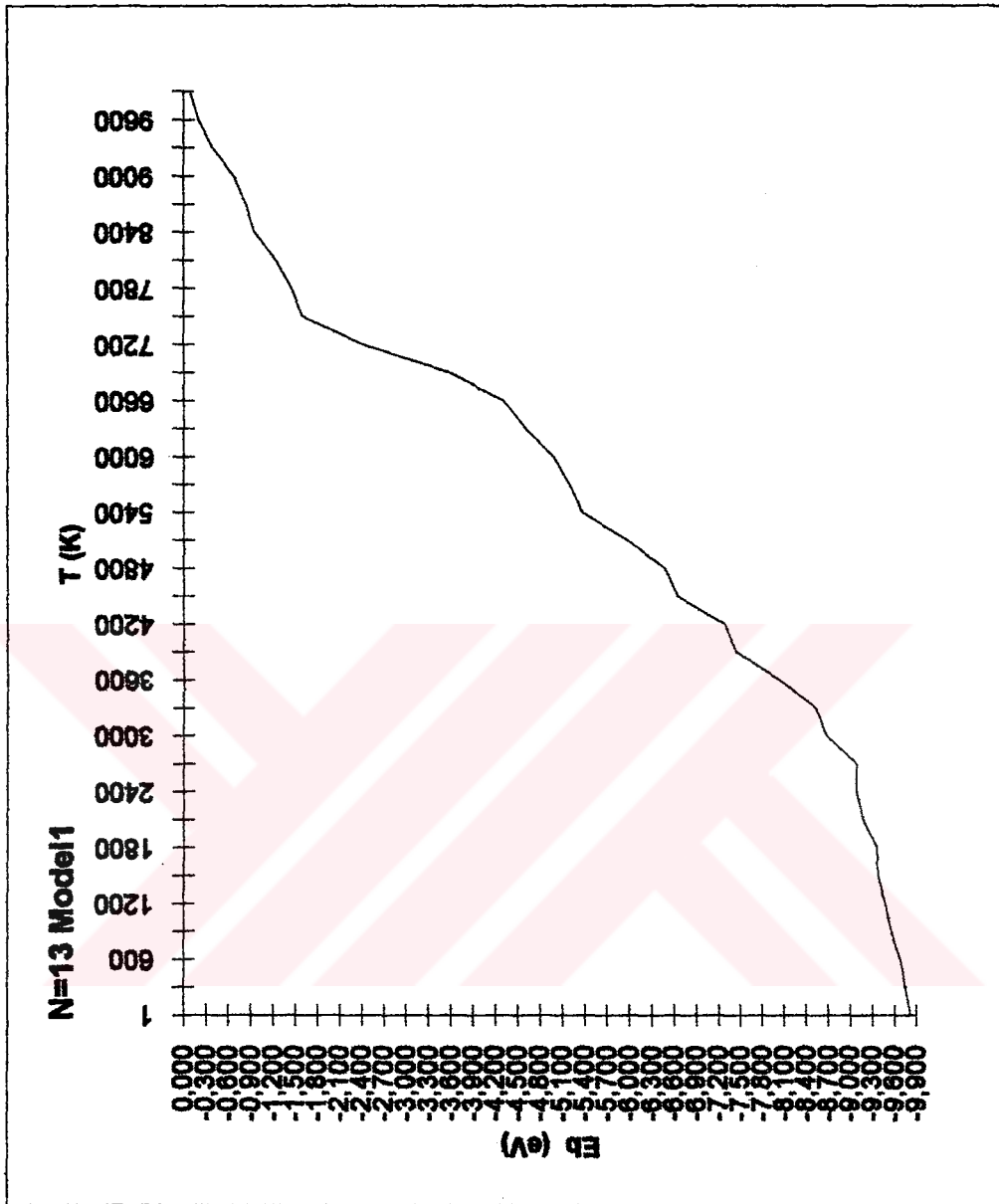


Figure 4.23: The variation of average interaction energy, E_b (in eV), as a function of temperature for $n = 13$ cluster by using model 1.

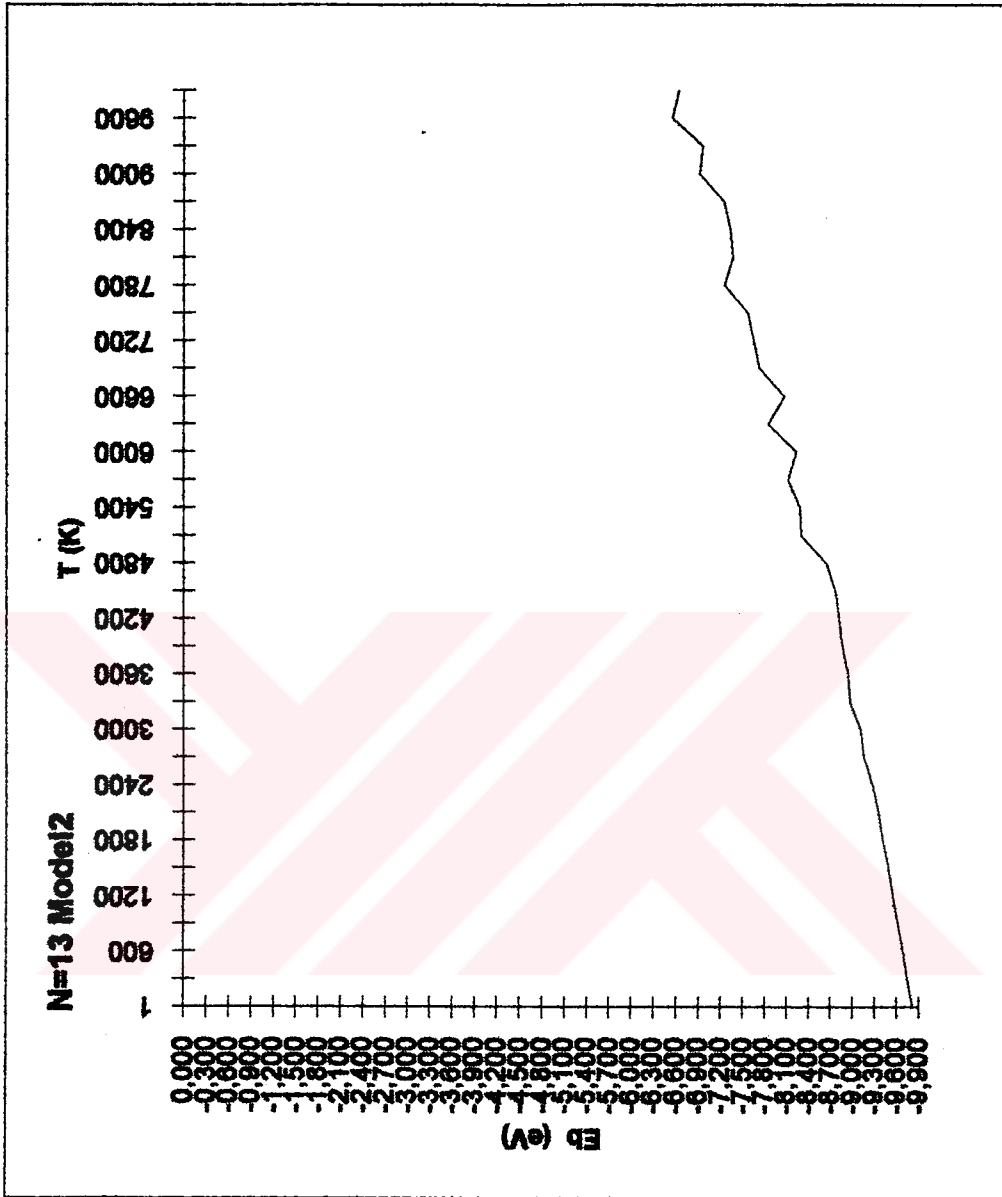


Figure 4.24: The variation of average interaction energy, E_b (in eV), as a function of temperature for $n = 13$ cluster by using model2.

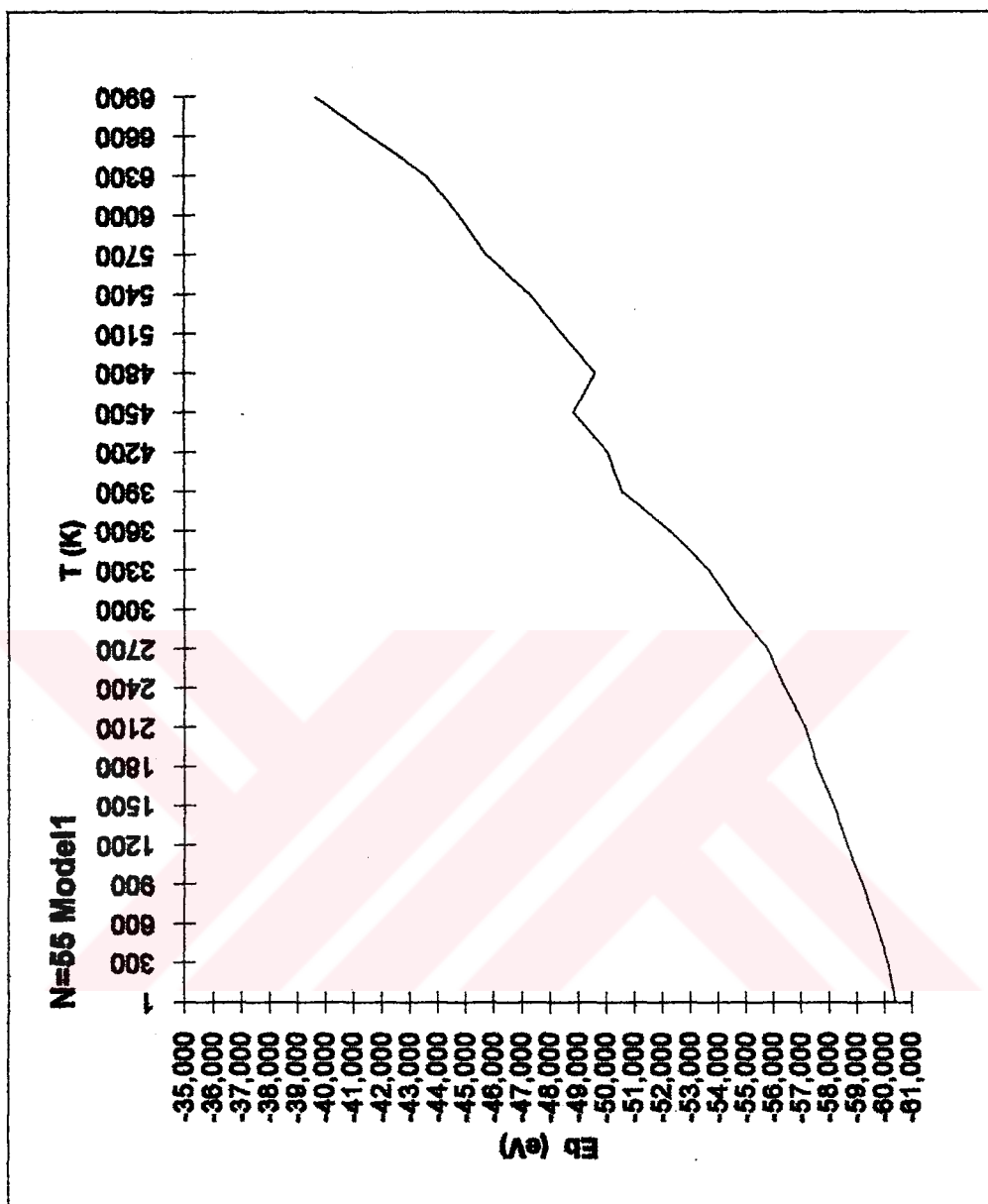


Figure 4.25: The variation of average interaction energy, E_b (in eV), as a function of temperature for $n = 55$ cluster by using model1.

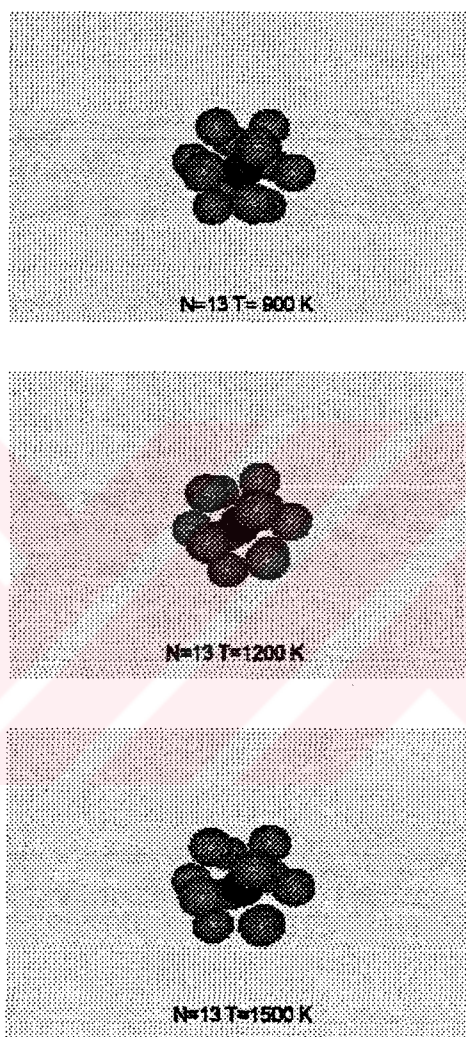


Figure 4.26: The distortions in structure for $n = 13$ cluster between $T = 900 K$ and $T = 1500 K$.

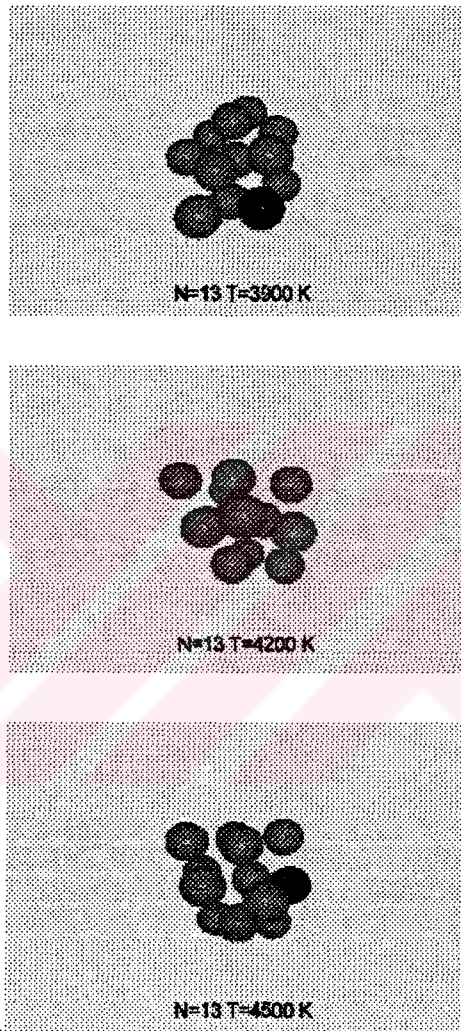


Figure 4.27: The distortions in structure for $n = 13$ cluster between $T = 3900 K$ and $T = 4500 K$.

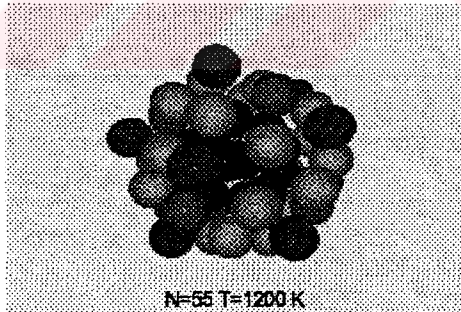
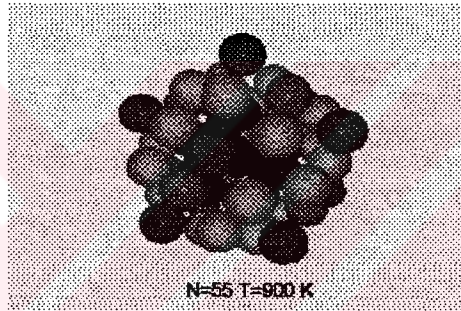
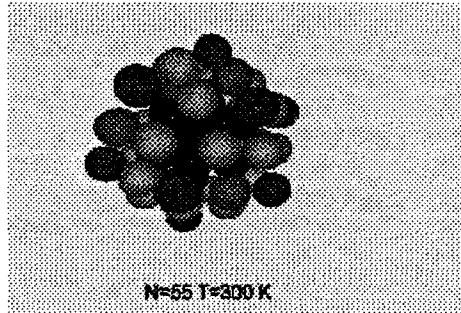


Figure 4.28: The distortions in structure for $n = 55$ cluster between $T = 300 K$ and $T = 1200 K$.

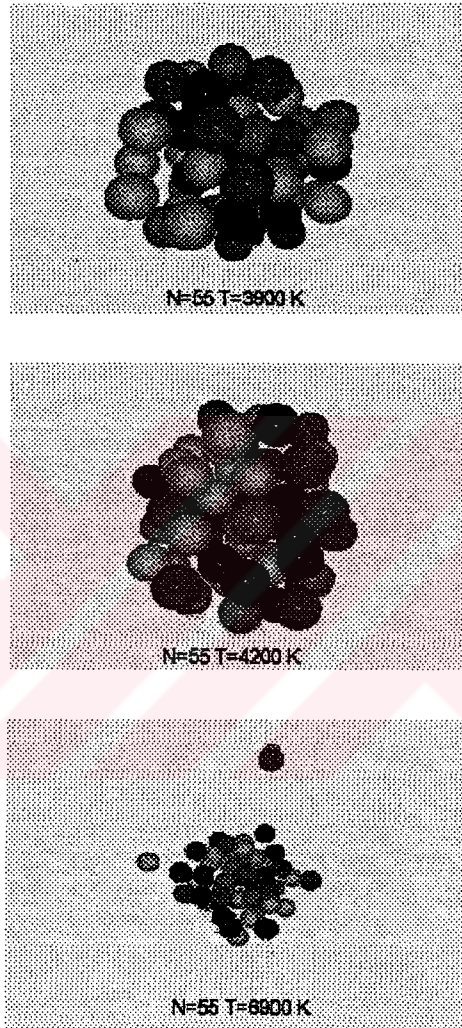


Figure 4.29: The distortions in structure for $n = 55$ cluster between $T = 3900 K$ and $T = 6900 K$.

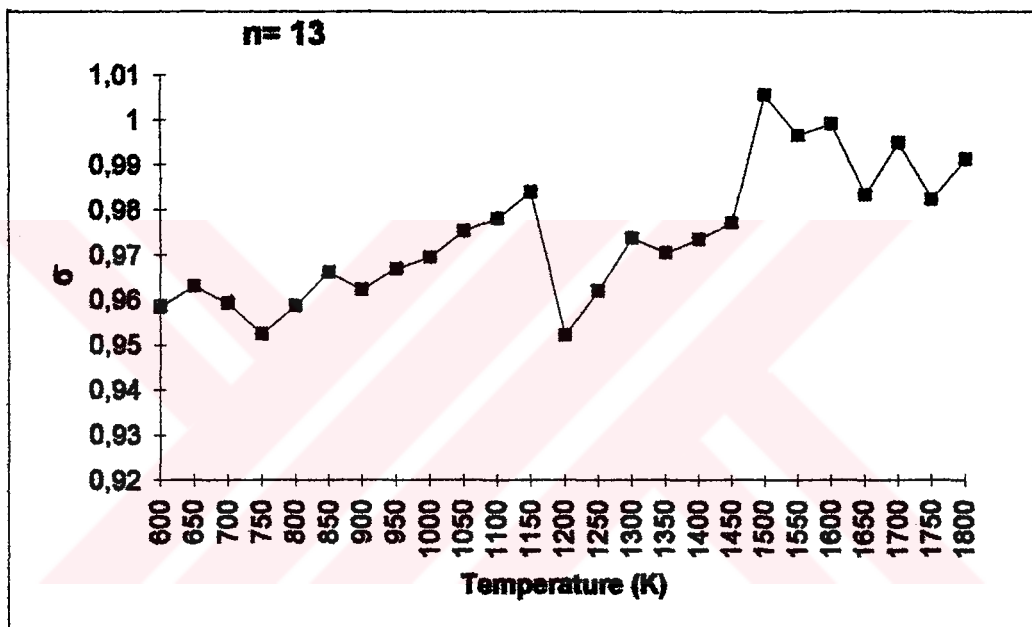


Figure 4.30: Standard Deviation (σ) versus Temperature (in K) for $n = 13$ cluster.

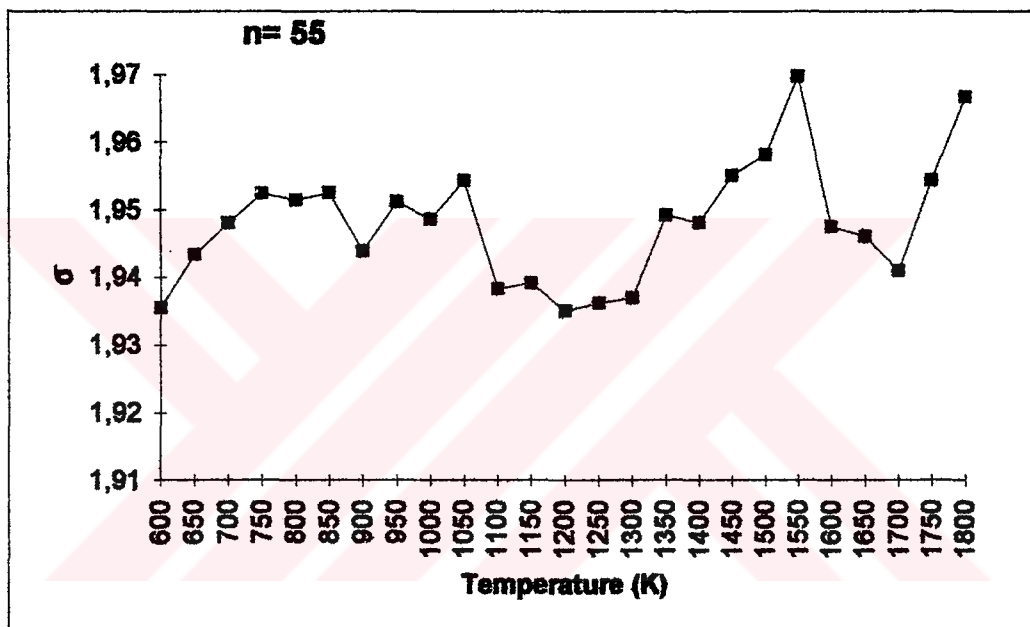


Figure 4.31: Standard Deviation (σ) versus Temperature (in K) for $n = 55$ cluster.

Table 4.5: Calculated melting points for $n = 13$, $n = 55$ clusters and inner shells of $n = 55$ cluster.

clusters and shells	Melting Temperature (in K)
$n = 13$	1350
N_1 of $n = 55$	1275
N_2 of $n = 55$	1250
N_3 of $n = 55$	975
$n = 55$	975

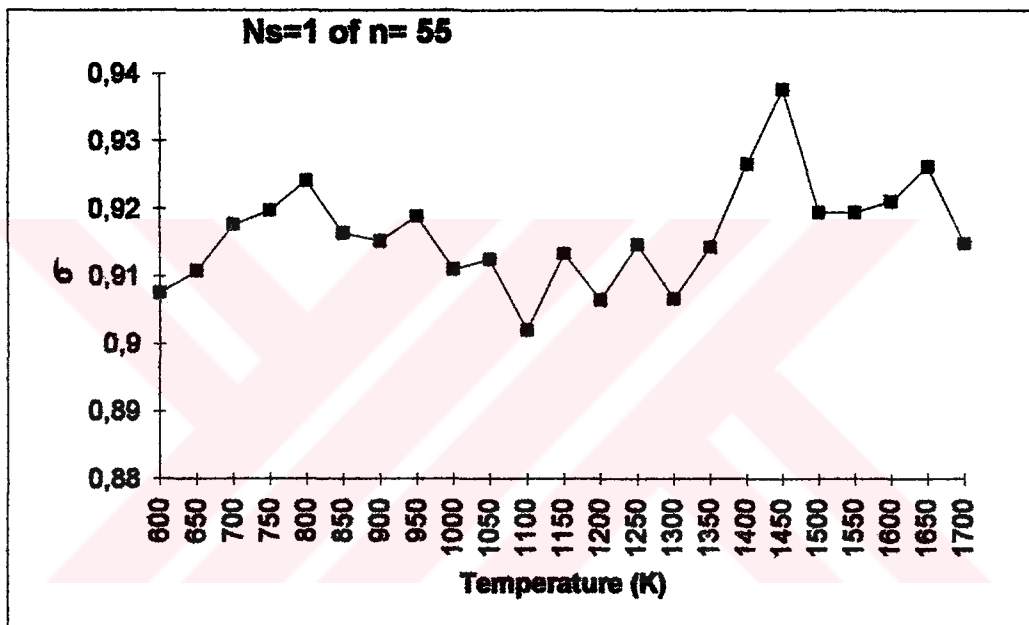


Figure 4.32: Standard Deviations of N_1 of $n = 55$ cluster versus Temperature (in K).

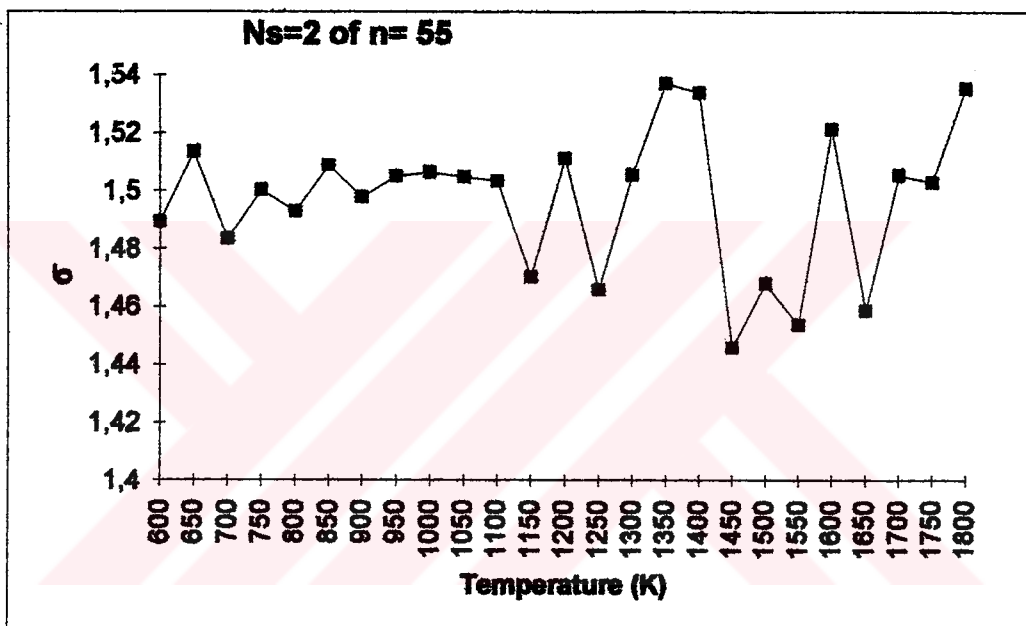


Figure 4.33: Standard Deviations of N_2 of $n = 55$ cluster versus Temperature (in K).

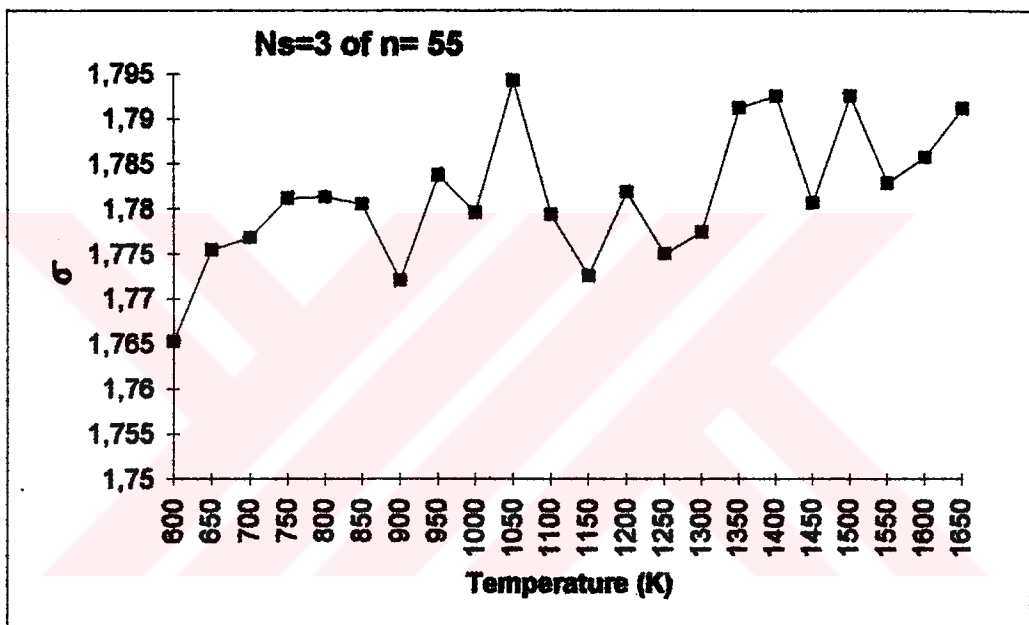


Figure 4.34: Standard Deviations of N_3 of $n = 55$ cluster versus Temperature (in K).

CHAPTER 5

CONCLUSION & DISCUSSION

In this study, the structural stability and energetics of Cu_n ($n = 13 - 135$) shell-like structured clusters (generated from fcc crystal structure) at temperatures $T = 1 \text{ K}$ and $T = 300 \text{ K}$ and the melting behaviour of clusters $n = 13$ and $n = 55$ have been investigated by using the Molecular-Dynamics technique.

In the simulation an empirical potential energy function (PEF) proposed by Erkoç has been used, although it is formed from pair-interactions only, it also contains many-body effects. The PEF satisfies the bulk cohesive energy, and the bulk stability condition exactly. It also gives the elastic constants and bulk modulus of copper. This PEF was applied for the stability and energetics of copper clusters. Therefore the present PEF satisfies some cluster and bulk properties of copper.

For microclusters, there is a relation such as; $r_0 < r < d_{nn}$ where r_0 is the dimer separation, d_{nn} is the nearest-neighbour distance in the crystal and r is the nearest-neighbor distance in the cluster. We have found that the order changes for shell-like clusters. The analogy is such that; $r_0 < d_{nn} < r$. It has been found that the average interaction energy per atom, Φ/n , in the cluster

decreases and reaches an asymptotic value as the cluster size increases. The calculated values for Ideal, $T = 1\text{ K}$ and $T = 300\text{ K}$ are given in Table 4.4. Delley *et al.* [74] calculated the binding energies for fcc Cu_{13} and Cu_{79} clusters by using self-consistent one-electron local-density theory. The calculated binding energy per atom of Cu_{13} , Cu_{79} are 2.19 and 3.03 eV/atom, respectively. In the work of Xie *et al.* [75], comparative calculations of the binding energy of relaxed closed-shell clusters of icosahedral and cuboctahedral (authors prefer it to refer as fcc because of its generation from fcc crystal) symmetry were reported. The atoms are presumed to interact via the Aziz-Chen (HFD-C) pair potential. The binding energy per atom of Cu_{13} , Cu_{55} for fcc structure are 3.04 and 4.59 eV/atom, respectively. As it is seen from Table 4.4, our results and above results do not suit numerically and even they do not agree with each other. The reason for that is, the nature of calculations are very different from each other (such as in Delley *et al.*'s work; *ab initio*, in Xie *et al.*'s work; Monte Carlo, in our work; Molecular Dynamics simulation methods). However, the ratio of results is taken as a criteria of comparison. The ratios for Delley *et al.*'s, Xie *et al.*'s and for our work are given in Table 5.1 for a quantitative comparison. The results are comparable with each other. There is no available data for copper clusters $n = 19, 43, 87, 135$ in the literature.

Table 5.1: The ratios of average interaction energy per atom for Cu_n ($n = 13, 55, 79$) clusters.

Clusters	Delley [74]	Xie [75]	Present calculations		
			Ideal	$T = 1 K$	$T = 300 K$
Cu_{13}/Cu_{55}	—	0.6626	0.6494	0.6875	0.6871
Cu_{13}/Cu_{79}	0.7228	—	0.6014	0.6646	0.6501

We have melted $n = 13, 55$ clusters as the second part of our work. We chose $n = 13$ cluster because of its high symmetry, and $n = 55$ cluster to see the melting behaviour of a multi-shell structure. We took the fluctuations of standard deviations of interatomic distances between the central atom and atoms surrounding it as the definition of melting[76]. The corresponding values for $n = 13$ and $n = 55$ clusters are $T = 1350 K$ and $T = 975 K$, respectively. Garcia *et al.* have carried out molecular dynamic simulation to study the structure and melting of Cu_{13} cluster by using the Voter and Chen version of the embedded-atom model. Cluster has structure based on icosahedral packing. Their result for melting is $T(Cu_{13}) = 1041 K$. The corresponding experimental bulk melting temperature is $T(Cu) = 1358 K$ [48]. There is no available data for $T(Cu_{55})$ in the literature. It has been found that the melting temperature decreases as cluster size increases, and for clusters with multishell structures melting starts from the outermost shell.

The *ab initio* calculations for Copper clusters (particularly microclusters) [74, 77-87] do not totally agree with each other. Therefore, parameterised

models seem to become feasible in this respect, but the choice of potential energy function is an important task, since simulation results show strong dependence on the functional form of the potential to avoid the shortcomings in small-cluster research based on the computer simulation.

We investigated cluster properties of Copper element. But, it is also possible to investigate different elements by using present computer program and present PEF, if the PEF is parameterised with respect to the properties of the element. It may also be proposed to study on the nucleation phenomena and radiation damage on clusters as future works by using present computer program with small modifications.

REFERENCES

- [1] J. L. Gole, *Metal Clusters* ed M Moskovits (New York: Wiley-Interscience) pp 131–84 (1986).
- [2] J. Jortner, *Ber. Bunsenges., Phys. Chem.* **88**, 188–201 (1984).
- [3] J. Koutecky, and P. Fantucci, *Chem. Rev.* **86**, 539–87 (1986a); also *Z. Phys. D* **3**, 147–53 (1986b).
- [4] G. M. Pound, *Metall. Trans. A* **16**, 487–502 (1985).
- [5] F. O. Hagen, *Z. Phys. D* **4**, 291–9 (1987).
- [6] J. Farges, M. F. De Feraudy, B. Raoult and G. Torchet *Surf. Sci.* **156**, 370–8 (1985).
- [7] M. Gillet, A. Renou, *Surf. Sci.* **106**, 27–34 (1981).
- [8] K. Hermann, H. J. Hass and P. S. Bagus *Z. Phys. D* **3**, 159–66 (1986).
- [9] R. C. Baetzold, *Surf. Sci.* **106**, 243–50 (1981).
- [10] T. Halicioglu and C. W. Bauschlicher, Jr., *Rep. Prog. Phys.* **51**, 883–921, (And references therein) (1988).
- [11] S. Bjørnholm, *Contemporary Physics* **31**, 309–24 (1990).
- [12] M. D. Morse and R. E. Smalley, *Ber. Bunsenges., Phys. Chem.* **88**, 228–33 (1984).
- [13] R. S. Bowles, J. J. Kolstad, J. M. Calo and R. P. Andres, *Surf. Sci.* **106**, 117–24 (1981).
- [14] A. W. Castleman, Jr., and R. G. Keesee, *Chem. Rev.* **86**, 589–618 (1986).
- [15] P. Joyes, J. Van de Wallr and C. Colliex, *Ultramicroscopy* **20**, 65–70 (1986).
- [16] J. Gspann, *Ber. Bunsenges., Phys. Chem.* **88**, 256–7 (1984); also *Z. Phys. D* **3**, 143–5 (1986).
- [17] M. M. Kappes, E. Schumacher, *Surf. Sci.* **156**, 1–7 (1985).
- [18] R. G. Keesee, R. Sievert and A. W. Castleman, Jr., *Ber. Bunsenges., Phys. Chem.* **88**, 273–4 (1984).

- [19] M. Arnold, J. Kowalski, G. zu Putlitz, T. Stehlin and F. Trager, *Surf. Sci.* **156**, 149–56 (1985).
- [20] W. Schulze, F. Frank, K. P. Charle and B. Tesche, *Ber. Bunsenges., Phys. Chem.* **88**, 263–5 (1984).
- [21] E. Schumacher, M. M. Kappes, K. Marti, P. Radi, M. Schar and B. Schmidhalter, *Ber. Bunsenges., Phys. Chem.* **88**, 220–8 (1984).
- [22] C. S. Feigerle, R. R. Corderman, S. V. Bobashev and W. C. Lineberger, *J. Chem. Phys.* **74**, 1580–98 (1981).
- [23] A. E. Stevens, C. S. Feigerle and W. C. Lineberger, *J. Chem. Phys.* **78**, 5420–31 (1983).
- [24] L. Bartell, *Chem. Rev.* **86**, 493–505 (1986).
- [25] E. Kay, *Z. Phys. D* **3**, 251–62 (1986).
- [26] H. Poppa, D. Moorhead and K. Heinemann, *Thin Solid Films* **128**, 251–67 (1985).
- [27] P. Gallezot, *Metal Clusters* ed M Moskovits (New York: Wiley-Interscience) pp 219–48 (1986); also *Catalysis Science and Technology* vol 5, ed J. R. Anderson and M. Boudart (Berlin: Springer) ch 4, pp 221–89 (1983).
- [28] D. L. Doering, H. Poppa and J. T. Dickinson, *J. Vac. Sci. Technol.* **20**, 827–30 (1982).
- [29] R. D. Moorhead, H. Poppa and K. Heinemann, *J. Vac. Sci. Technol.* **17**, 248–50 (1980).
- [30] J. J. Metois, K. Heinemann and H. Poppa, *Thin Solid Films* **41**, 197–207 (1977).
- [31] R. Anton, H. Poppa, *Proc. 10th Int. Congr. on Electron Microscopy, Hamburg* (Deutsche gesellschaft für Elektronen Mikroskopie) pp 511–2 (1982).
- [32] C. L. Fu, A. J. Freeman, E. Wimmer and M. Weinert, *Phys. Rev. Lett.* **54**, 2261–4 (1985).
- [33] B. K. Rao, P. Jena, *Phys. Rev.* **32**, 2058–69 (1985).
- [34] W. L. Brown, R. R. Freeman, K. Raghavachari and M. Schluter, *Science* **235**, 860–5 (1987).
- [35] T. L. Beck, J. Jellinek and R. S. Berry, *J. Chem. Phys.* **87**, 545–54 (1987).

- [36] J. D. Honeycut and H. C. Andersen, *J. Phys. Chem.* **91**, 4950–63 (1987).
- [37] L. D. Heidi, J. Jellinek and R. S. Berry, *J. Chem. Phys.* **86**, 6456–64 (1987).
- [38] J. Jellinek, T. L. Beck, and R. S. Berry, *J. Chem. Phys.* **84**, 2783–94 (1986).
- [39] N. Quirke and P. Sheng, *Chem. Phys. Lett.* **110**, 63–6 (1984).
- [40] R. D. Eppers, J. Kaelberer, *J. Chem. Phys.* **66**, 5112–6 (1977).
- [41] J. M. Ziman, *Principles of The Theory of Solids* (Cambridge University Press) section 6.10, (1965).
- [42] O. Sinanoğlu, *Adv. Chem. Phys.* **12**, 283 (1967).
- [43] C. Hoheisel, *Phys. Rev. A* **23**, 1998 (1981).
- [44] J. N. Murrell, S. Carter, S. C. Farantos, P. Huxley and A. J. C. Varandas, *Molecular Potential Energy Functions* (Willey), (1984).
- [45] Ş. Erkoç, *Z. Phys. D* **32**, 257–260 (1994).
- [46] Ş. Erkoç, *Phys. Status Solidi* **171**, 317 (1992).
- [47] M. D. Morse, *Chem. Rev.* **86**, 1049 (1986).
- [48] C. Kittel, *Introduction to Solid State Physics* 5th edition (New York: Wiley) (1976).
- [49] N. Metropolis, A. W. Rosenbluth, M. N. Rosenbluth, A. H. Teller and E. Teller, *J. Chem. Phys.* **21**, 1087 (1953).
- [50] B. J. Alder, T. E. Wainwright, *J. Chem. Phys.* **27**, 1208 (1957).
- [51] B. J. Alder, T. E. Wainwright, *Phys. Rev.* **127**, 359 (1962).
- [52] G. N. Vineyard, J. B. Gibson, A. N. Goland and M. Milgram, *Phys. Rev.* **120**, 1229 (1960).
- [53] A. Rahman, *Phys. Rev.* **136A**, 405 (1964).
- [54] L. Verlet, *Phys. Rev.* **159**, 98 (1967).
- [55] A. Rahman and F. H. Stillinger, *J. Chem. Phys.* **55**, 3336 (1971).
- [56] E. Clementi, H. Popkie and H. Kistenmacher, *J. Chem. Phys.* **59**, 1325 (1973).

- [57] O. Matsuoka, E. Clementi and M. Yoshimine, *J. Chem. Phys.* **64**, 1351 (1976).
- [58] A. Nordsieck, *Math. Comput.* **16**, 22 (1962).
- [59] G. W. Gear, *Numerical Initial Value Problems in Ordinary Differential Equations* Chap. 9 (Englewood Cliffs, NJ: Prentice Hall) (1971).
- [60] D. J. Evans, *Mol. Phys.* **34**, 317 (1977).
- [61] H. J. C. Berendsen, J. P. Ryckaert and G. Ciccotti, *J. Comput. Phys.* **23**, 327 (1977).
- [62] J. P. Valleau and G. M. Torrie, *J. Comput. Phys.* **23**, 187 (1977).
- [63] D. Frenkel and A. J. C. Ladd, *J. Chem. Phys.* **81**, 3188 (1984).
- [64] S. No e, *Molecular Dynamics Simulations* ed F. Yonezawa, (Berlin: Springer-Verlag) pp 11-19 (1990).
- [65] J. J. Erpenbeck and W. W. Wood, *Modern Theoretical Chem. Vol. 6, Statistical Mechanics Part B: Time Dependent Processes* Ed. Bruce J. Berne (Plenum Press, New York 1977).
- [66] D. Beeman, *J. Comput. Phys.* **20**, 130-9 (1976).
- [67] D. J. Evans and G. P. Morris, *Comput. Phys. Rep.* **1**, 297-343 (1984).
- [68] D. W. Heermann, *Computer Simulation Methods in Theoretical Physics* (Berlin: Springer-Verlag 1990).
- [69] J. Kushick and B. J. Berne *Modern Theoretical Chem. Vol. 6, Statistical Mechanics Part B: Time Dependent Processes* Ed. Bruce J. Berne (Plenum Press, New York 1977).
- [70] W. W. Wood and J. J. Erpenbeck, *Ann. Rev. Phys. Chem.* **27**, 319-48 (1976).
- [71] F. James, *Rep. Prog. Phys.* **43**, 1145-89 (1980).
- [72] G. Bhanot, *Rep. Prog. Phys.* **51**, 429-57 (1988).
- [73] L. T. Wille, *Chem. Phys. Lett.* **133**, 405-10 (1987).
- [74] B. Delley, D. E. Ellis, E. J. Baerends and D. Post, *Physical Review B* **27**, 2132-44 (1983).
- [75] J. Xie, J. A. Northby, D. L. Freeman and J. D. Doll, *J. Chem. Phys.* **91**, 612-19 (1989).

- [76] J. Garcia-Rodeja, C. Rey, L. J. Gallego and J. A. Alonso, *Physical Review B* **49**, 8495–98 (1994).
- [77] H. Tatewaki, E. Miyoshi and T. Nakamura, *J. Chem. Phys.* **76**, 5073 (1982).
- [78] R. C. Baetzold, *J. Phys. Chem.* **80**, 1504 (1976).
- [79] A. B. Anderson, *J. Chem. Phys.* **68**, 1744 (1978).
- [80] C. Bachman, J. Demuynck and A. Veilard, *Faraday Symp. R. Soc.* **14**, 170 (1980).
- [81] C. Bachman, J. Demuynck and A. Veilard, *Growth and Properties of Metal Clusters* Ed. J. Bourdon, (Amsterdam: Elsevier) (1980).
- [82] J. Flad, G. Igel-Mann, H. Preuss and H. Stoll, *Chem. Phys.* **90**, 257 (1984).
- [83] G. H. Jeung, M. Pelissier and J. C. Barthelat, *Chem. Phys. Lett.* **97**, 369 (1983).
- [84] S. C. Richtmeier, J. L. Gole and D. A. Dixon, *Proc. Natl. Acad. Sci. U.S.A.* **77**, 5611 (1980).
- [85] E. Miyoshi, H. Tatewaki and T. Nakamura, *Int. J. Quantum Chem.* **23**, 1201 (1983).
- [86] J. Demuynck, M. Rohmer, A. Strich and A. Veilard, *J. Chem. Phys.* **75**, 3443 (1981).
- [87] D. Post, E. Baerends, *J. Surf. Sci.* **116**, 177 (1982).
- [88] F. W. Sears and G. L. Salinger, *Thermodynamics, Kinetic Theory, and Statistical Thermodynamics* 3rd edition (Massachusetts: Addison-Wesley) pp 302–62 (1986).

APPENDIX A

ACRONYMS

AES	Auger electron spectroscopy
CI	Configuration interaction
CPU	Central processing unit
EM	Energy minimization
EXAFS	Extended x-ray absorption fine structure
HREM	High-resolution electron microscopy
LEED	Low-energy electron diffraction
LMIS	Liquid-metal ion source
MCSCF	Multi-configurational self-consistent field
MC	Monte Carlo
MD	Molecular Dynamics
MO	Molecular orbital
NEMD	Non-equilibrium Molecular Dynamics
RED	Radial electron distribution
REM	Reflection electron microscopy

SCF	Self-consistent field
SIMS	Secondary ion mass spectroscopy
STED	Scanning transmission electron diffraction
STEM	Scanning transmission electron microscopy
TEM	Transmission electron microscopy
TOFMS	Time-of-flight mass spectroscopy
TPD	Temperature programmed desorption
UHV	Ultrahigh vacuum
UPS	Ultraviolet photoelectron spectroscopy
WF	Work function
XPS	X-ray photoelectron spectroscopy

APPENDIX B

MAXWELL–BOLTZMANN VELOCITY DISTRIBUTION

B.1 The distribution of molecular velocities

The first step is to calculate the partition function,

$$Z = \sum_j g_j \exp(-\mathcal{E}_j/kT) \quad (\text{B.1})$$

where \mathcal{E}_j is the energy and g_j is the degeneracy of each level.

$$\mathcal{E}_j = \frac{N_j^2 h^2 V^{-2/3}}{8m}, \quad n_j^2 = n_x^2 + n_y^2 + n_z^2 \quad (\text{B.2})$$

Total number of possible states in all energy levels up to and including the energy \mathcal{E}_j ,

$$G_j = \frac{1}{8} \left(\frac{4}{3} \pi n_j^3 \right) \quad (\text{B.3})$$

Total number of possible states between \mathcal{E}_j and $\mathcal{E}_j + \Delta\mathcal{E}_j$ (degeneracy of the macrolevel),

$$\Delta G_j = \frac{\pi}{2} n_j^2 \Delta n_j \quad (\text{B.4})$$

inserting the expressions for ΔG_j and \mathcal{E}_j , we have

$$\begin{aligned} Z &= \sum_j \Delta G_j \exp(-\mathcal{E}_j/kT) = \frac{\pi}{2} \sum_j n_j^2 \exp\left(-\frac{h^2 V^{-2/3}}{8mkT} n_j^2\right) \Delta n_j \\ &= \frac{\pi}{2} \int_0^\infty n_j^2 \exp\left(-\frac{h^2 V^{-2/3}}{8mkT} n_j^2\right) dn_j = V \left(\frac{2\pi mkT}{h^2} \right)^{3/2} \end{aligned} \quad (\text{B.5})$$

The partition function therefore depends both on the temperature T and the volume V , which corresponds to the general extensive variable. The importance of the partition function Z is that in Maxwell–Boltzmann and classical statistics, all the thermodynamic properties of a system can be expressed in terms of $\ln Z$ and its partial derivatives. According to Maxwell–Boltzmann Distribution,

$$\Delta \mathcal{N}_j = \frac{N}{Z} \Delta G_j \exp(-\mathcal{E}_j/kT) \quad (\text{B.6})$$

where N is the total number of molecules with energies up to and including the energy \mathcal{E}_j ; $\Delta \mathcal{N}_j$ is the average occupation number of the macrolevel and

$$\mathcal{E}_j = \frac{n_j^2 h^2 V^{-2/3}}{8m} = \frac{1}{2} m v_j^2, \quad \Delta G_j = \frac{\pi}{2} n_j^2 \Delta n_j \rightarrow \Delta G_v = \frac{4\pi m^3 V}{h^3} n^2 \Delta v$$

It follows from these equations that, in velocity space,

$$\Delta \mathcal{N}_v = \frac{4N}{\sqrt{\pi}} \left(\frac{m}{2kT} \right)^{3/2} v^2 \exp\left(-\frac{mv^2}{2kT}\right) \Delta v \quad (\text{B.7})$$

The quantity \mathcal{N}_v represents the average total number of molecules with all speeds up to and including v , and $\Delta \mathcal{N}_v$ is the average number with speeds between v and v and Δv .

It is helpful to visualize the distribution in terms of ‘velocity space’. Imagine that at some instant a vector v is attached to each molecule representing its velocity in magnitude and direction, and that these vectors are then transferred to a common origin, resulting in a sort of spiny sea urchin. The velocity of each molecule is represented by the point at the tip of the corresponding velocity vector. Fig. B.1 shows one octant of this velocity space.

Geometrically speaking, the quantity \mathcal{N}_v represents the average total number of representative points within a sphere of radius v , and $\Delta\mathcal{N}_v$ the number within a spherical shell of radius v and thickness $\Delta\mathcal{N}_v$.

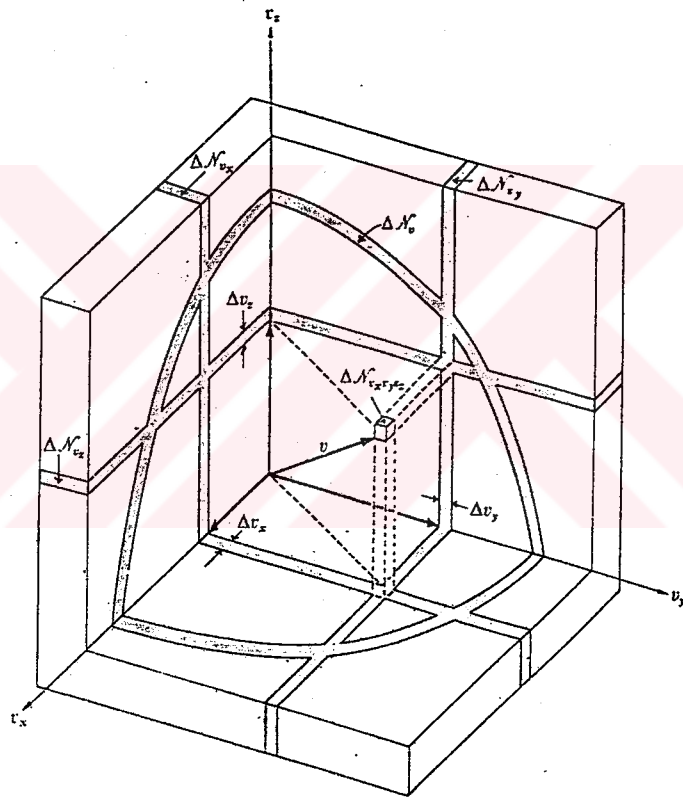


Figure B.1: Diagram of velocity space.

The coefficient of $\Delta\mathcal{N}_v$ in Eq.(B.7), equal to the ratio $\frac{\Delta\mathcal{N}_v}{\Delta v}$, depends only on the magnitude of v , or on the speed. It is called the Maxwell–Boltzmann speed distribution function and is plotted as a function of v on Fig. B.2.

If velocity space is subdivided into spherical shells of equal thickness, the speed v_m at which the distribution function is a maximum is the radius of that spherical shell which includes the largest number of representative points. The speed v_m is called the most probable speed. To find its value, we take the first derivative of the distribution function with respect to v and set it equal to zero $d\mathcal{N}_v/dv = 0$.

$$v_m = \sqrt{\frac{2kT}{m}} \quad (\text{B.8})$$

The distribution function can now be expressed more compactly in terms of v_m ,

$$\Delta\mathcal{N}_v = \frac{4N}{\sqrt{\pi}v_m^3} v^2 \exp\left(-\frac{v^2}{v_m^2}\right) \Delta v \quad (\text{B.9})$$

$$\frac{\Delta\mathcal{N}_v}{\Delta v} = \frac{4N}{\sqrt{\pi}v_m^3} v^2 \exp\left(-\frac{v^2}{v_m^2}\right) \quad (\text{B.10})$$

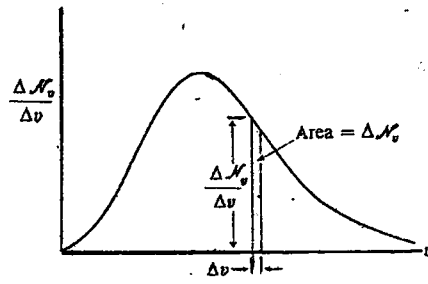


Figure B.2: Graph of Maxwell–Boltzmann speed distribution function.

Average or arithmetic mean speed is,

$$\begin{aligned}\bar{v} &= \frac{1}{N} \sum v \Delta N_v \\ &= \frac{4}{\sqrt{\pi} v_m^3} \int_0^{\infty} v^3 \exp\left(-\frac{v^2}{v_m^2}\right) dv = \frac{2}{\sqrt{\pi}} v_m = \sqrt{\frac{8kT}{\pi m}}\end{aligned}\quad (\text{B.11})$$

The root-mean-square speed is

$$\begin{aligned}v_{rms} &= \sqrt{\bar{v}^2} = \left(\frac{1}{N} \sum v^2 \Delta N_v\right)^{1/2} = \left(\frac{4}{\sqrt{\pi} v_m^3} \int_0^{\infty} v^4 \exp\left(-\frac{v^2}{v_m^2}\right) dv\right)^{1/2} \\ &= \frac{3}{2} v_m = \sqrt{\frac{3kT}{m}}\end{aligned}\quad (\text{B.12})$$

In summary, we have

$$v_m = \sqrt{\frac{2kT}{m}}, \quad v = \sqrt{\frac{2.55kT}{m}}, \quad v_{rms} = \sqrt{\frac{3kT}{m}} \quad (\text{B.13})$$

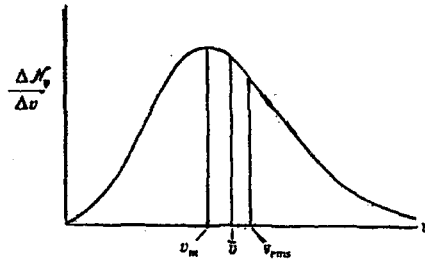


Figure B.3: Most probable (v_m), arithmetic mean (\bar{v}), and the root-mean-square (v_{rms}) speeds.

The three speeds are shown in Fig. B.3,

The relative magnitudes of the three, at a given temperature, are [88]

$$v_m : \bar{v} : v_{rms} \equiv 1 : 1.128 : 1.224.$$

B.2 Algorithm for Maxwell Velocity Distribution

- Setting initial velocities via randomly distribution of velocities around v_m
- According to the Kinetic Theory,

$$\frac{1}{2}m\bar{v}^2 = \frac{3}{2}kT$$

It is needed to find the most probable velocity v_m , so using the relations,

$$\bar{v}^2 = \frac{3kT}{m}$$

$$v_{rms} = \sqrt{v^2} = \sqrt{\frac{3kT}{m}}$$

$$v_m = \sqrt{\frac{2}{3}}v_{rms}$$

So, the expression for the most probable velocity v_m ,

$$v_m = \sqrt{\frac{2}{3}}v^2$$

- Then normalization of this vector by dividing $\sqrt{3}$, that is the assumption of the radius of velocity space constituted by equal components in magnitude, giving the radius of the spherical shell which includes the largest number of representative points,

- Using a random number generator giving values $(-1, 1)$,

$$\text{Velocity Components} \equiv (v_{mean} - v_{mean} * \text{RandomNumber})$$

velocities (in all directions) distributed by using this procedure,

- Finding the averages values for each distributed velocity directions

$$\bar{v}_x, \bar{v}_y, \bar{v}_z$$

- Dividing each components to radius vector which is, $((\bar{v}_x)^2 + (\bar{v}_y)^2 + (\bar{v}_z)^2)^{1/2}$, then finding direction cosines which are useful for scaling distributed velocities with respect to the given temperature

- Calculating kinetic energy and temperature with respect to the calculated v_m as,

$$\text{Kinetic Energy} \equiv \frac{1}{2}M\left(\frac{3}{2}v_m^2\right)$$

- Calculating the scaling factor,

$$(Temperature\ given / Temperature\ calculated)^{1/2} \equiv ScaleFactor$$

- Redistributing the initial speeds with respect to scaling factor by multiplying each component by scale factor,

$$v_i = (|\vec{v}^i|) * ScaleFactor, \quad i = 1, 2, 3$$

- Subtracting from average values $v_i - \bar{v}_i$ gives differences from averages, these are new scales and adding to each component of each atom gives new speeds of each atom in each direction,

- Finding the averages for each distributed velocity directions $\bar{v}_x, \bar{v}_y, \bar{v}_z$ as,

$$v_i = \frac{1}{N} \sum_{\alpha} v_{\alpha}^i$$

- Finding the radius vector by,

$$v_m = ((\bar{v}_x)^2 + (\bar{v}_y)^2 + (\bar{v}_z)^2)^{1/2}$$

- Finding kinetic energy by,

$$Kinetic\ Energy \equiv \frac{1}{2} M \left(\frac{3}{2} v_m^2 \right)$$

- Finding calculated temperature,

$$TE_{calc} = \frac{KE_{calc}}{\frac{3}{2} k_B}$$

Since it has the same value with the given temperature, the initial velocities have been distributed successfully for each atom in all directions.

APPENDIX C

ALGORITHM AND FLOWCHART OF THE PROGRAM

C.1 Algorithm

- Reading initial coordinates from the input file,
- Setting initial velocities according to the Maxwell-Boltzmann velocity distribution,
- Calculating initial potential energy of the system (at time step n),
- Starting MD steps,
- Calculating velocity and position of the atoms using the velocity summed form of Verlet Algorithm (NVE MD Velocity Form)[68],
- Calculating force by present coordinates (at time step n),
- Computing the positions at time step $n + 1$ as,
$$r_i(n + 1) = r_i(n) + \Delta v_i(n) + \frac{1}{2}m\Delta^2 F_i(n)$$
- Storing the force values ($F_i(n)$) at time step n ,
- Calculating force by new coordinates (at time step $n + 1$),

- Computing the velocities at time step $n + 1$ as,

$$v_i(n + 1) = v_i(n) + \frac{\Delta}{2m} [F_i(n + 1) + F_i(n)]$$

- Calculating the potential energy of the system at time step $n + 1$,
- Calculating the temperature that the system reached by summing the kinetic energy of each atom,

$$\sum_i^N \frac{1}{2} m v_i^2 = \frac{3}{2} k_B N T \rightarrow T = \frac{3m}{k_B N} \sum_i^N v_i^2 \equiv T_{CALC}$$

- Scaling the velocities by scale factor,

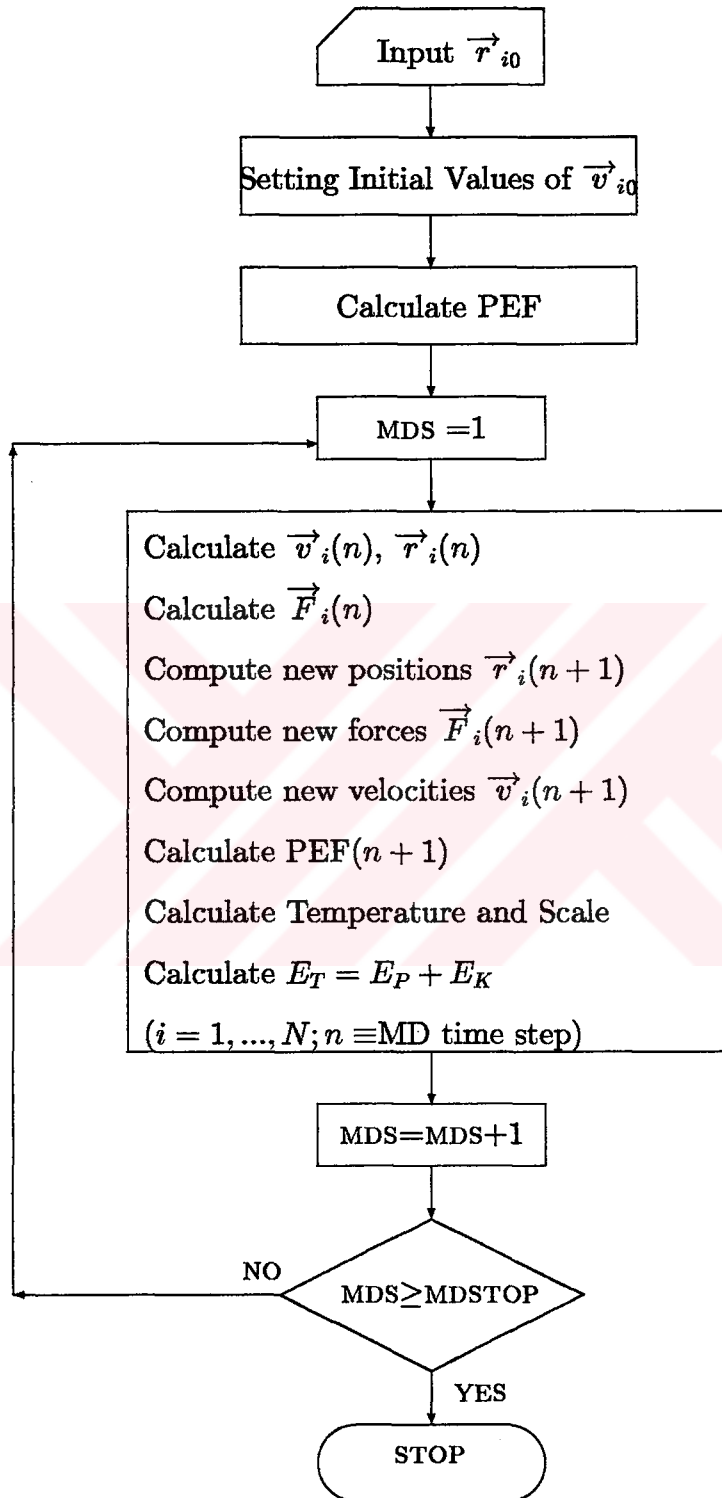
$$SCFAC \equiv \sqrt{TE / T_{CALC}} \rightarrow \text{multiplying by each speed component}$$

→ makes the system having initially given temperature

- Calculating total energy,

← Starting the procedure again until the initially given step number reached.

C.2 Flowchart



APPENDIX D

DETERMINATION OF ΔT

It is found by using dimer values of Copper (see Figure II.1).

$$r_0 = 2.22 \text{ \AA}$$

$$\mathcal{E}_0 = 2.01 \text{ eV}$$

$$m = 63.546 \text{ atom gr/mol}$$

An equality for Δt can be found by using the equation;

$$\frac{1}{2}mv^2|_{\Delta x=r_0} = \mathcal{E}_0 = \frac{1}{2}m \left(\frac{\Delta x}{\Delta t} \right)^2 \quad (\text{D.1})$$

such as;

$$\Delta t = \sqrt{\frac{mr_0^2}{2\mathcal{E}_0}} \quad (\text{D.2})$$

with numerical values for Copper;

$$\Delta t = \sqrt{\frac{63.546 \frac{\text{atom}}{6.0225 \times 10^{23} \text{ atom}} * 10^{-3} \text{ kg} * (2.22 * 10^{-10} \text{ m})^2}{2 * 2.01 * 1.6 * 10^{-19} \frac{\text{eV}}{\text{eV}} \text{ kg} \frac{\text{m}^2}{\text{s}^2}}} = 89.91572728 * 10^{-15} \text{ s}$$

From the experience of scientists working in this field, it was determined that 1/100 of the calculated Δt is the value works well in MD simulations.

Therefore the determined molecular dynamics time step value in this work is;

$$DT = 0.8991572728 * 10^{-15} \text{ s.}$$